

# Cycles-L: A coupled, 3-D, land surface, hydrologic, and agroecosystem landscape model

Yuning Shi<sup>1</sup>, Felipe Montes<sup>2</sup>, and Armen R Kemanian<sup>2</sup>

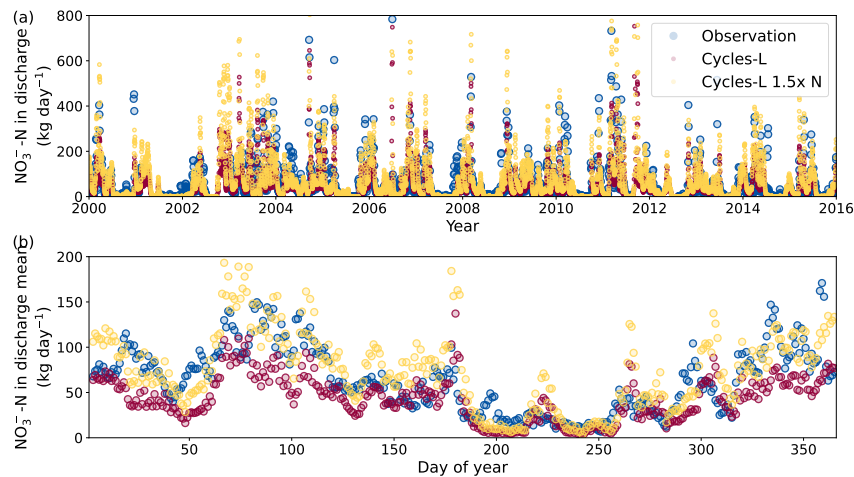
<sup>1</sup>The Pennsylvania State University

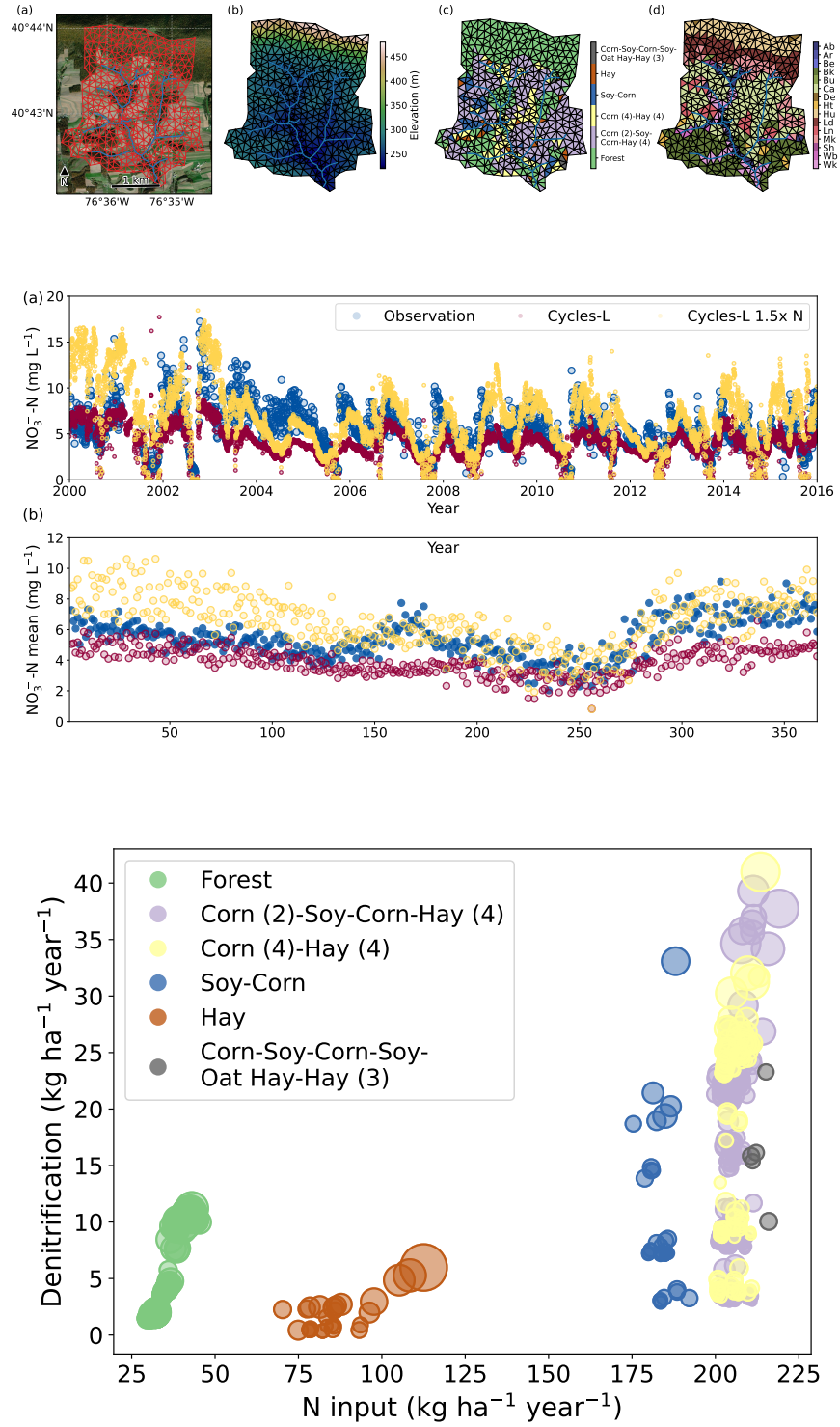
<sup>2</sup>Pennsylvania State University

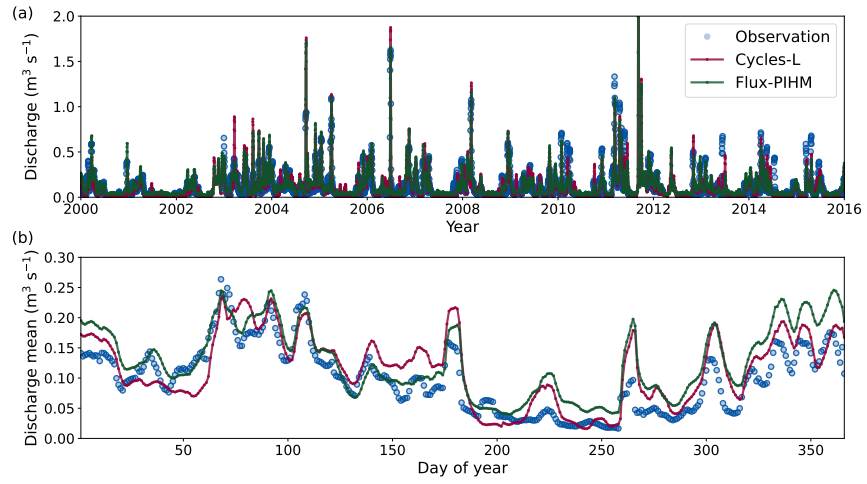
November 21, 2022

## Abstract

Managing landscapes to increase agricultural productivity and environmental stewardship requires spatially distributed models that can integrate data and operate at spatial and temporal scales that are intervention-relevant. This paper presents Cycles-L, a landscape-scale, coupled agroecosystem hydrologic modeling system. Cycles-L couples a 3-D land surface hydrologic model, Flux-PIHM, with a 1-D agroecosystem model, Cycles. Cycles-L takes the landscape and hydrology structure from Flux-PIHM and most agroecosystem processes from Cycles. Consequently, Cycles-L can simulate landscape level processes affected by topography, soil heterogeneity, and management practices, owing to its physically-based hydrologic component and ability to simulate horizontal and vertical transport of mineral nitrogen (N) with water. The model was tested at a 730-ha agricultural experimental watershed within the Mahantango Creek watershed in Pennsylvania. Cycles-L simulated well stream water discharge and N exports (Nash-Sutcliffe coefficient 0.55 and 0.58, respectively), and grain crop yield (root mean square error 1.01 Mg ha<sup>-1</sup>), despite some uncertainty in the accuracy of survey-based input data. Cycles-L outputs are as good if not better than those obtained with the uncoupled Flux-PIHM (water discharge) and Cycles (crop yield) models. Model predicted spatial patterns of N fluxes clearly show the combined control of crop management and topography. Cycles-L spatial and temporal resolution fills a gap in the availability of analytical models at an operational scale relevant to evaluate costly strategic and tactical interventions *in silico*, and can become a core component of tools for applications in precision agriculture, precision conservation, and artificial intelligence-based decision support systems.







1 **Cycles-L: A coupled, 3-D, land surface, hydrologic, and**  
2 **agroecosystem landscape model**

3 **Yuning Shi<sup>1</sup>, Felipe Montes<sup>1</sup>, and Armen R. Kemanian<sup>1</sup>**

4 <sup>1</sup>Department of Plant Science, The Pennsylvania State University

5 **Key Points:**

- 6 • Cycles-L is a coupled agroecosystem hydrologic modeling system that couples an  
7 agroecosystem model with a 3-D land surface hydrologic model  
8 • Cycles-L simulated well stream discharge, grain crops yield, and nitrogen exports  
9 in the stream at a 730-ha agricultural experimental watershed  
10 • Cycles-L can simulate landscape level processes affected by topography, soil het-  
11 erogeneity, and management practices

## Abstract

Managing landscapes to increase agricultural productivity and environmental stewardship requires spatially distributed models that can integrate data and operate at spatial and temporal scales that are intervention-relevant. This paper presents Cycles-L, a landscape-scale, coupled agroecosystem hydrologic modeling system. Cycles-L couples a 3-D land surface hydrologic model, Flux-PIHM, with a 1-D agroecosystem model, Cycles. Cycles-L takes the landscape and hydrology structure from Flux-PIHM and most agroecosystem processes from Cycles. Consequently, Cycles-L can simulate landscape level processes affected by topography, soil heterogeneity, and management practices, owing to its physically-based hydrologic component and ability to simulate horizontal and vertical transport of mineral nitrogen (N) with water. The model was tested at a 730-ha agricultural experimental watershed within the Mahantango Creek watershed in Pennsylvania. Cycles-L simulated well stream water discharge and N exports (Nash-Sutcliffe coefficient 0.55 and 0.58, respectively), and grain crop yield (root mean square error 1.01 Mg ha<sup>-1</sup>), despite some uncertainty in the accuracy of survey-based input data. Cycles-L outputs are as good if not better than those obtained with the uncoupled Flux-PIHM (water discharge) and Cycles (crop yield) models. Model predicted spatial patterns of N fluxes clearly show the combined control of crop management and topography. Cycles-L spatial and temporal resolution fills a gap in the availability of analytical models at an operational scale relevant to evaluate costly strategic and tactical interventions *in silico*, and can become a core component of tools for applications in precision agriculture, precision conservation, and artificial intelligence-based decision support systems.

## 1 Introduction

Managing landscapes to increase agricultural productivity and environmental stewardship requires understanding and representing landscape attributes with ever increasing fidelity. The ability to represent *in silico* the spatial variability and temporal dynamics of water and nutrient flows in such landscapes through modeling tools can help significantly in the design of cost-effective interventions in the realms of precision agriculture, precision conservation, or watershed management (Beaujouan et al., 2001; Booker et al., 2014; Stöckle et al., 2014). These modeling tools are known as spatially distributed. Two features are critical for these models to be applicable. First, they must integrate the wealth of real-time data incoming from *in situ* sensors, proximal sensing from unmanned aerial vehicles (UAVs) and terrestrial vehicles (UTVs), remote sensing from satellites, and constantly refined terrain and surface data (e.g., the Soil Survey Geographic Database or SSURGO, and the National Land Cover Database or NLCD), and meteorological data such as the Global Land Data Assimilation System (GLDAS; Rodell et al., 2004) and Europe’s World Climate Research Program Coordinated Regional Downscaling Experiment (EURO-CORDEX; Jacob et al., 2014). Second, these models must operate at a scale of relevance to represent interventions and with minimal supervision, so that they do not become “mathematical marionettes” (Kirchner, 2006). There are to our knowledge only partial efforts at integrating models and data in this fashion. This paper presents the model Cycles-L, where L stands for landscape. Cycles-L integrates Flux-PIHM (Shi et al., 2013), a 3-D energy and hydrology model, and the Cycles agroecosystem model (Kemanian et al., 2022).

One-dimensional cropping system models are established tools for planning and decision making in agriculture systems with low spatial variability and high quality input data (e.g., Boote et al., 2010; Stöckle & Kemanian, 2020; Zhai et al., 2020). Applications of these 1-D models in precision agriculture lag behind their promise (Stafford, 2000) because, among other limitations (Zhai et al., 2020), the representation of both static and dynamic properties that vary spatially is limited. Although these models are often used in a gridded way in an attempt to represent spatial heterogeneity (e.g., Saarikko, 2000; Batchelor et al., 2002; Basso et al., 2007), their 1-D nature and lack of lateral water and

64 nutrient transport among grids significantly limits their ability to represent nonlinear-  
65 ities in water and nutrient availability caused by topography and soil heterogeneity. An  
66 additional impedance is that using these models in a way that enriches decision-making  
67 requires substantial competence (Confalonieri et al., 2016).

68 There have been, however, efforts at developing models that represent spatial and  
69 temporal variability in a semi-distributed fashion in non-agricultural (Tague & Band,  
70 2004) and agricultural landscapes without resorting to costly numerical solutions of wa-  
71 ter flow in landscapes. For example, the Soil Water Assessment Tool (SWAT; Arnold et  
72 al., 1998) and the Agricultural Policy EXtender (APEX; Gassman et al., 2010) divide  
73 the model domain into subareas (e.g., Hydrological Response Units, or HRUs) by ter-  
74 rain or soil attributes. Within HRUs, processes are simulated using the core of the 1-D  
75 EPIC model (J. R. Williams, 1990). In the SWAT model, HRUs do not interact; an HRU’s  
76 water, nutrient, and sediment runoff contributions to the corresponding watershed out-  
77 let are represented through HRU-specific delivery ratios. However, sediment generation  
78 and delivery, for example, are not equally scaled to the HRU area, which causes output  
79 variations solely dependent on the HRU generation scheme (E. Chen & Mackay, 2004).  
80 In the APEX model, the HRUs (or subareas) are hydrologically connected, but the land-  
81 scape segmentation methodology is *ad hoc* (Kemanian et al., 2009), calibration require-  
82 ments are substantial (X. Wang et al., 2011), and the calibration parameters are not nec-  
83 essarily robust (Francesconi et al., 2014; Van Liew et al., 2017). These challenges are not  
84 unique to these modeling systems but are easily overlooked and difficult to grasp with-  
85 out substantial training, as alluded to in general by Confalonieri et al. (2016). Further-  
86 more, models that aggregate large spatial scales can represent some processes very well  
87 (Arnold et al., 1998; Koch et al., 2016), but cannot represent highly non-linear processes  
88 controlled by within-subarea heterogeneity in topography, soil, and landcover. Both Stöckle  
89 and Kemanian (2020) and Tenreiro et al. (2020) concluded that among the most promis-  
90 ing areas for improvement of current cropping system models is the representation of land-  
91 scape processes that affect surface inflow and subsurface lateral flows of water and other  
92 constituents. Although efforts in this direction have been underway for decades (e.g. Beau-  
93 jouan et al., 2001), the usage of spatially-distributed models remains limited. A robust,  
94 scale-independent formulation of routing is desirable to dispel uncertainty and to reduce  
95 dependence on local calibration.

96 Advances in computational power and modeling techniques have paved the way to  
97 the development of coupled agroecosystem hydrologic models. The Precision Agricultural-  
98 Landscape Modeling System (PALMS; Molling et al., 2005) combines an enhanced 2-D  
99 diffusive wave runoff model with a 1-D biophysical model based on the Integrated Bio-  
100 sphere Simulator (IBIS; Foley et al., 1996; Kucharik et al., 2000). PALMS has been used  
101 to simulate crop and erosion processes (e.g., Molling et al., 2005; Bonilla et al., 2007, 2008),  
102 and connected to other crop models (Booker et al., 2014, 2015). Although the PALMS  
103 grids are hydrologically connected at the surface, horizontal distribution of subsurface  
104 water is empiric and subsurface lateral flow is not explicitly simulated. Ward et al. (2018)  
105 presented a spatially distributed and 3-D hydrologic cropping system model, CropSyst-Microbasin  
106 (CS-MB), which added the Soil Moisture Routing model-based subsurface lateral flow  
107 to CropSyst. The model was tested in a 10.9-ha watershed growing rainfed wheat in the  
108 Inland Pacific Northwest, USA, showing promising potential to simulate field-scale spa-  
109 tial variability of water distribution and grain yield. The kinematic assumption used by  
110 this model, i.e., the hydraulic gradient for subsurface water flow follows the land slope  
111 rather than the water table slope, limits its application on gentle slopes (Wigmosta &  
112 Lettenmaier, 1999).

113 While crop production is a primary target in landscape management, more com-  
114 prehensive models are needed to track dynamic processes that reshape the landscape such  
115 as soil and sediments erosion and deposition (Pineux et al., 2017) and changes in soil or-  
116 ganic carbon stocks (Baker et al., 2007), as well as to represent the provision of ecosys-

tem services determined by landscape diversity (Frank et al., 2012). Processes need to be represented along the continuum of soil, groundwater, and streams. For example, nitrogen (N) is both a critical plant macronutrient needed to reach high crop yield and a source of pollution (McLellan et al., 2018). Within the Chesapeake Bay Watershed (CBW), Ator and Garcia (2016) estimated that of the total N input to the CBW as fertilizer, biological N fixation, and N deposition, up to 18% is delivered to tidal waters or stored in the stream, 19% is harvested, and 45% is lost as denitrification. Most N losses occur when there is a large mismatch between N extraction in harvest and N applied as fertilizer (Woodbury et al., 2018; McLellan et al., 2018). Furthermore, high N losses as denitrification point to potentially high and unreported losses of  $\text{N}_2\text{O}$  if denitrification is incomplete (Saha et al., 2021). Opportunities exist therefore to reduce N losses in a cost-effective and environmentally friendly fashion, and taking advantage of these opportunities can greatly benefit from robust modeling and diagnostic tools.

The objectives of this paper are to present Cycles-L, a coupled agroecosystem hydrologic modeling system, and to demonstrate its use through a case study. We tested Cycles-L at an agricultural experimental watershed, WE-38, that is nested in the larger watershed of the Mahantango Creek in Pennsylvania. The long-term records of discharge and water quality, together with the surveys of crop rotations, make WE-38 an ideal site for testing Cycles-L. We evaluate and discuss the simulated discharge, stream  $\text{NO}_3^-$ -N concentrations, and crop yield with observations and county-level surveys, to showcase the degree of fidelity and utility of Cycles-L for landscape level analysis.

## 2 Cycles-L Components Description

### 2.1 Flux-PIHM

Flux-PIHM is a spatially distributed land surface hydrologic model that integrates the Penn State Integrated Hydrologic Model (PIHM; Qu & Duffy, 2007; Bhatt et al., 2014) and the Noah land surface model component (F. Chen & Dudhia, 2001; Ek et al., 2003). Flux-PIHM simulates 3-D soil, groundwater, and river hydrology, along with the surface energy balance with high spatial resolution, representing land surface and hydrological variability resulting from soil, landcover, and topographic heterogeneity (Shi et al., 2015). Flux-PIHM is the core of other terrestrial biogeochemistry (Shi et al., 2018; Zhi et al., 2022) and reactive transport models (Bao et al., 2017).

In Flux-PIHM, the land surface is decomposed into unstructured triangular grids for optimal representation of local heterogeneities (topography, soil, and land cover), river channels, and watershed boundaries. River channels are represented by rectangular elements (Tarboton et al., 1991). Water transport between soil, ground, and river follows PIHM (Qu & Duffy, 2007). PIHM uses de Saint-Venant (1871) equations to compute channel (1-D) and surface (2-D) water flow. Infiltration at the air-soil interface is calculated using the properties of the top 10 cm of soil following Darcy’s law. In the subsurface, the prismatic and triangular volume is divided into water saturated and unsaturated zones. Unsaturated water transport only occurs vertically. In the saturated zone, groundwater flow is horizontal with dynamic coupling to the unsaturated zone across the water table, governed by Darcy’s law. The hydrologic equations at each model grid are discretized to ordinary differential equations (ODEs), which are assembled within the boundaries of the domain, and solved simultaneously using the CVODE ODE solver (Hindmarsh et al., 2005). The land surface component of Flux-PIHM is adapted from the Noah land surface model (F. Chen & Dudhia, 2001; Ek et al., 2003), and is coupled to PIHM by exchanging water table depth, infiltration rate, water table position, net precipitation rate, and evapotranspiration rate between the two components. The land surface component simulates surface energy balance, snow melt, interception, and drip. In the land surface component, the subsurface is divided into layers with fixed thickness. By default, the soil layer thickness increases from 0.11 m for the first layer to 0.38 m for the 10th

168 layer (Shi et al., 2015). The number of soil layers can be reduced, and the thickness of  
 169 the deepest layer can be adjusted to match the depth to bedrock. If the bedrock is deeper  
 170 than the total thickness of 10 soil layers, one additional layer is added as needed. While  
 171 PIHM only simulates infiltration rate, lateral subsurface flow rate, and position of wa-  
 172 ter table for all model grids, these variables are used as boundary conditions by the land  
 173 surface model to calculate transport within the unsaturated zone using the Richards equa-  
 174 tion. A recent development is adding a topographic solar radiation module to Flux-PIHM  
 175 (Shi et al., 2018). Flux-PIHM is now the core landscape hydrology model for multiple  
 176 modeling systems. Detailed descriptions of PIHM and Flux-PIHM are provided by Qu  
 177 and Duffy (2007), and Shi et al. (2013, 2014, 2018).

## 178 2.2 Cycles

179 Cycles is a one-dimensional process-based multi-year and multi-species agroecosys-  
 180 tem model (Kemanian et al., 2022). Cycles evolved from C-Farm (Kemanian & Stöckle,  
 181 2010) and shares biophysical modules with CropSyst (Stöckle et al., 2014). Cycles sim-  
 182 ulates the water and energy balance, the coupled cycling of carbon (C) and N, and plant  
 183 growth at daily time steps. Evapotranspiration is calculated based on the Penman-Monteith  
 184 equation. Transpiration is modulated by temperature, crop root distribution, soil wa-  
 185 ter potential, and plant hydraulic properties (Campbell, 1985). Plant development is de-  
 186 termined by thermal time, and plant growth is based on solar radiation interception (light  
 187 limited) or the realized transpiration (water limited) based on stomatal optimization the-  
 188 ory (Cowan, 1978, 1982; Katul et al., 2009). Soil organic C and N cycling are based on  
 189 saturation theory (Kemanian & Stöckle, 2010; Pravia et al., 2019). The model can sim-  
 190 ulate a wide range of perturbations of biogeochemical processes caused by management  
 191 practices such as tillage, irrigation, organic and inorganic nutrient additions, annual and  
 192 perennial crop selections, crop harvests as grain or forages, polycultures, relay cropping,  
 193 and grazing. Cycles can simulate unlimited plant species as specified by the user.

## 194 2.3 Cycles-L

195 Cycles-L (Fig. 1) takes the landscape and hydrology structure from Flux-PIHM and  
 196 most agroecosystem processes from Cycles. The surface energy balance and soil hydrol-  
 197 ogy are simulated as in Flux-PIHM, except for plant water uptake, hydraulic lifting, and  
 198 the water balance of surface plant residues, which use Cycles' algorithms. Hydrologic pro-  
 199 cesses are simulated with a sub-daily time step (usually  $\sim 10^0$  minute, dynamic). Fol-  
 200 lowing Cycles, each soil layer has texture- and organic matter-dependent hydraulic prop-  
 201 erties. However, when activating landscape hydrology, the properties of the soil profile  
 202 are averaged preserving total soil mass and porosity to allow solving for vertical and lat-  
 203 eral fluxes using Flux-PIHM. Biogeochemical processes are simulated with a daily time  
 204 step independently for each soil layer. Tillage operations allow mixing all components  
 205 of the soil layers affected by tillage. The one-dimensional Cycles model is integrated into  
 206 every Flux-PIHM model grid, therefore each model grid can be assigned with a unique  
 207 land cover or crop rotation.

208 A solute transport module is used to simulate subsurface nutrient transport. This  
 209 model is the same as the subsurface transport in Flux-PIHM-BGC (Shi et al., 2018), and  
 210 is used to calculate total solute flowing in or out of a model grid:

$$211 \quad V_i \frac{d}{dt} (\Theta_i C_i) = \sum_j (-q_{ij} C_{ij}) + F, \quad (1)$$

212 where  $V_i$  is the subsurface prism volume of grid  $i$  ( $\text{m}^3$ ),  $C_i$  is the subsurface mineral N  
 213 concentration ( $\text{kg m}^{-3}$ ),  $\Theta_i$  is the volumetric soil water content ( $\text{m}^3 \text{m}^{-3}$ ),  $q_{ij}$  is the lat-  
 214 eral water flow at the subsurface between grid  $i$  and its neighbor at edge  $j$  ( $\text{m}^3 \text{s}^{-1}$ ), and  
 215  $F$  is a source/sink term of the corresponding solute ( $\text{kg s}^{-1}$ ). In Cycles-L, the source/sink

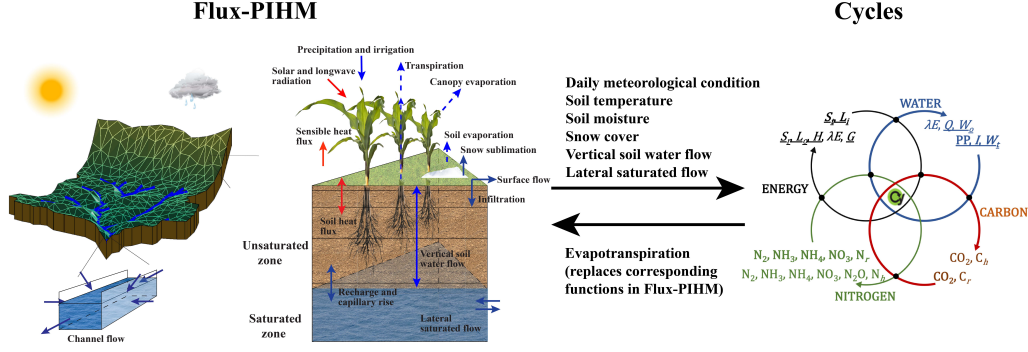


**Figure 1.** Schematic illustration of land surface and hydrologic processes simulated by Flux-PIHM; energy, water, carbon (C) and nitrogen (N) cycles simulated by Cycles with fluxes in and out for each component; and the coupling between Flux-PIHM and Cycles. For Cycles, the nodes at the arrows' intersections represent interactions between cycles;  $S_t$  and  $L_i$  are incoming shortwave and longwave radiation,  $S_r$  and  $L_o$  are outgoing shortwave and longwave radiation,  $H$ ,  $\lambda E$ , and  $G$  are sensible, latent, and ground heat fluxes,  $PP$  is precipitation,  $I$  is irrigation,  $W_t$  is capillary rise,  $Q$  is runoff,  $W_o$  is soil percolation or lateral flow,  $C_r$  and  $N_r$  are C and N changes caused by soil amendments, and  $C_h$  and  $N_h$  are harvested C and N. When coupled, the processes represented by dashed arrows in Flux-PIHM are simulated by Cycles, and the fluxes with underlines in Cycles are calculated by Flux-PIHM.

216 terms for mineral N are:

$$217 \quad \frac{d}{dt} \text{NO}_3^- \text{-N} = \text{NO}_3^- \text{-N}_f + \text{NO}_3^- \text{-N}_d + \text{NO}_3^- \text{-N}_{\text{nit}} + \text{NO}_3^- \text{-N}_{\text{imm}} \quad (2a)$$

$$218 \quad - \text{NO}_3^- \text{-N}_{\text{dnit}} - \text{NO}_3^- \text{-N}_{\text{pup}} - \text{NO}_3^- \text{-N}_l - \text{NO}_3^- \text{-N}_r$$

219 and

$$220 \quad \frac{d}{dt} \text{NH}_4^+ \text{-N} = \text{NH}_4^+ \text{-N}_f + \text{NH}_4^+ \text{-N}_d + \text{NH}_4^+ \text{-N}_{\text{min}}$$

$$221 \quad - \text{NH}_4^+ \text{-N}_{\text{nit}} - \text{NH}_4^+ \text{-N}_{\text{imm}} - \text{NH}_4^+ \text{-N}_{\text{pup}} - \text{NH}_3 \text{-N}_{\text{vol}} - \text{NH}_4^+ \text{-N}_l - \text{NH}_4^+ \text{-N}_r \quad (2b)$$

222 where subscript  $f$  is for fertilizer,  $d$  for deposition, nit for nitrification, imm for micro-  
 223 bial immobilization or microbial uptake, pup for plant uptake, dnit for denitrification,  
 224  $l$  for leaching or percolation,  $r$  for runoff, min for mineralization of organic compounds  
 225 with N (many), and vol for volatilization as  $\text{NH}_3$ -N. Note that  $\text{NO}_3^- \text{-N}_{\text{nit}}$  and  $\text{NH}_4^+ \text{-N}_{\text{nit}}$   
 226 are the same, and  $\text{NH}_4^+$  and  $\text{NO}_3^-$  are just N species identifiers. If the net water flow from  
 227 a grid is outward (net efflux from grid  $i$  to grid  $j$ ) then the mineral N concentration ( $C_{ij}$ )  
 228 of the water flow ( $q_{ij}$ ) is that of grid  $i$ :  $C_{ij} = C_i$ ; otherwise,  $C_{ij} = C_j$ . In Flux-PIHM,  
 229 horizontal water flow is restricted to the saturated zone. But this horizontal flow is cal-  
 230 ibrated to include the representation of lateral perched flow above unsaturated layers and  
 231 that flow can drag mineral N (M. R. Williams et al., 2015) or other solutes. This is dif-  
 232 ficult to predict because it depends on the mixing between water flowing through macro-  
 233 pores and water in the non-macropore soil matrix and the distribution of mineral N. To  
 234 account empirically for that transport, we tentatively assigned a weight function that  
 235 allows for mineral N transport from unsaturated layers. The weighting function is  $\frac{K_r}{D-d_z}$ ,  
 236 where  $K_r$  is the relative hydraulic conductivity (hydraulic conductivity divided by sat-  
 237 urated hydraulic conductivity),  $D$  is the total soil depth, and  $d_z$  is the depth of the cor-  
 238 responding soil layer. This function is applied to all soil layers when calculating the ave-  
 239 rage concentration of soil mineral N, to emulate the horizontal transport of mineral N

240 in the shallower depths with higher hydraulic conductivities. Due to the very low hy-  
 241 draulic conductivity of dry layers, they contribute little to mineral N transport.

242 At the beginning of each simulation day, land surface processes are calculated first  
 243 using the Noah land surface model. Note that in Cycles-L, Noah LSM evapotranspira-  
 244 tion functions are replaced by the corresponding Cycles functions. Cycles then applies  
 245 management operations and simulates vegetation, residue, and soil C and N processes,  
 246 using as input the daily meteorological conditions, soil temperature, soil moisture, and  
 247 snow cover informed by Flux-PIHM. Cycles passes evapotranspiration rate and N fluxes  
 248 as source/sink terms in water and N transport. Then, Flux-PIHM calculates the trans-  
 249 port of water and N for the entire domain using sub-daily time steps.

### 250 3 Site and data

#### 251 3.1 Description of the WE-38 watershed

252 The WE-38 watershed is a 7.3 km<sup>2</sup> first-order watershed within the Mahantango  
 253 Creek Watershed in Pennsylvania’s Northumberland county (Fig. 2a). Elevation ranges  
 254 from 503 m at the northernmost ridge to about 214 m near the southern outlet. The land  
 255 cover comprises cultivated land (55%), followed by forests (40%), pasture (3%), and de-  
 256 veloped area (2%). The watershed contains more than 300 farm fields. Surveys and in-  
 257 terviews were used to obtain field-specific operations (Veith et al., 2015) that documented  
 258 crop species, planting and harvesting dates, tillage tools and operation dates, and syn-  
 259 thetic fertilizer and animal manure application rates and dates. The watershed has been  
 260 the focus of rigorous research on agricultural management and monitoring of water qual-  
 261 ity (Pionke et al., 2000; Bryant et al., 2011; Buda et al., 2011; Church et al., 2011; Lu  
 262 et al., 2015; Veith et al., 2015), and long-term discharge and water quality measurements,  
 263 including NO<sub>3</sub><sup>-</sup>-N and NH<sub>4</sub><sup>+</sup>-N, are publicly available.

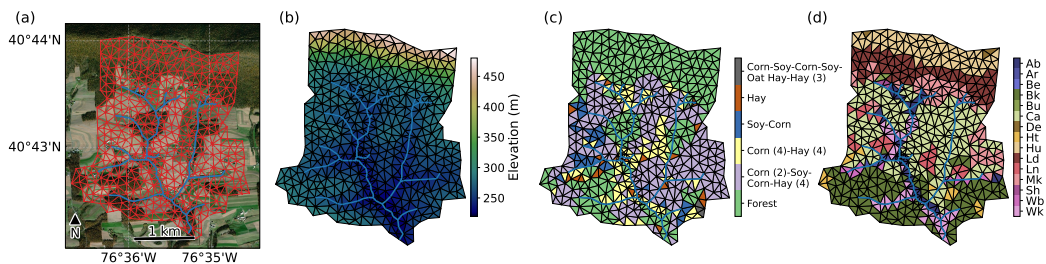


**Figure 2.** (a) WE-38 model domain projected onto an aerial photograph of the watershed. The red triangles represent the model grids and the blue lines represent river segments. (b) Surface elevation map of the WE-38 model domain. (c) Land use and crop rotations in the WE-38 model grids. (d) SSURGO soil map projected onto WE-38 model grids, with each color representing one unique soil type. The soil series are Albrights silt loam (Ab), Alvira silt loam (Ar), Bedington silt loam (Be), Berks channery silt loam (Bk), Buchanan channery loam (Bu), Calvin-Klinesville shaly silt loams (Ca), Dekalb very channery sandy loam (De), Hartleton channery silt loam (Ht), Hazleton and Clymer extremely stony sandy loams (Hu), Laidig and Meckesville extremely stony soils (Ld), Leck kill shaly silt loam (Ln), Meckesville silt loam (Mk), Shelmadine silt loam (Sh), Watson silt loam (Wb), and Weikert and Klinesville shaly silt loams (Wk).

### 3.2 Domain and model setup

The Cycles-L WE-38 model physical domain consists of 114 segments representing the stream network (average 98-m long) and 883 triangular grids (average 0.83 ha), of which 522 triangular grids are cropland (Fig. 2). The watershed drainage network was mapped using the Terrain Analysis Using Digital Elevation Models tool (TauDEM; Tarboton et al., 2009; Tarboton, 2015) on a digital elevation model (DEM) obtained from light detection and ranging (lidar) data and color orthophotography at horizontal and vertical resolutions of 0.5 and 0.15 m, respectively (Bryant et al., 2011). Afterwards, the drainage network was updated by overlapping the TauDEM analysis results with a geo-referenced orthomosaic of the watershed obtained from the Pennsylvania Spatial Data Access (PASDA, 2022).

To represent field operations, we converted the database used for WE-38 in Hirt et al. (2020) to Cycles-L inputs. This database aggregates field operations history by crop in the rotation. These rotations and associated field operations were projected on the Cycles-L WE-38 model domain (Fig. 2c). Model grids were assigned to one of six land uses: deciduous forest, a corn (2 years)-soybean-corn-hay (4 years) rotation, a corn (4 years)-hay (4 years) rotation, a soybean-corn rotation, a hay rotation, and a corn-soybean-corn-soybean-oat hay-hay (3 years) rotation. Hay was simulated as a mixture of 1/3 alfalfa and 2/3 orchardgrass. Deciduous forest is the most common land use type, while the corn (2 years)-soybean-corn-hay (4 years) rotation is the most common crop rotation. The operations for each crop are listed in Table 1.

To prevent an unrealistic rotation synchrony in grids with the same rotation, we randomly assigned a different starting point in the rotation to each grid within the assigned rotation. For example, for the model grids with the soybean-corn rotation, we randomly assigned half of those grids to start with soybean, and the other half to start with corn.

The soil properties texture, organic matter, and bulk density (by layer) were extracted from the SSURGO database projected to the model domain (Fig. 2d); 15 unique soil series were identified for the watershed. The meteorological forcing (precipitation, air temperature, humidity, wind speed, downward solar radiation, downward longwave radiation, and air pressure) were obtained from the North American Land Data Assimilation System Phase 2 (NLDAS-2; Xia et al., 2012) forcing data, which provides data at hourly time-step and is suitable for hydrologic simulations.

For model testing, annual crop yields were downloaded from the The United States Department of Agriculture (USDA) National Agricultural Statistics Service (NASS) at county level (Northumberland county) and compared with both Cycles 1-D and Cycles-L for the entire watershed.

The simulation period was 16 years from 0000 UTC 1 January 2000 to 0000 UTC 1 January 2016. Setting up the model requires spin-up to stabilize hydrological and biogeochemical soil properties. The spin-up process was divided into two, one for hydrology and one for soil variables. Because running Cycles-L is more computationally expensive than Flux-PIHM, we first ran Flux-PIHM for land surface hydrological parameter calibration and hydrological state spin-up. When running Flux-PIHM, the forest was simulated as the deciduous forest NLCD land cover type, the hay rotation was simulated as the pasture/hay land cover type, and all other crop rotations were simulated as the cultivated crop land cover type. The leaf area index (LAI) forcing was prescribed monthly climatological LAI that depends on land cover types. Flux-PIHM hydrologic and land surface parameters were manually calibrated using the observed discharge data from 2000 to 2011. Model parameters that affect horizontal flow and key parameters identified from Flux-PIHM sensitivity analyses (Shi et al., 2014; Xiao et al., 2019) were adjusted, including vertical and horizontal saturated hydraulic conductivities, vertical and

**Table 1.** Field operations for crops in the rotation. The N-P-K refers to the proportion of N, P, and K in the dry mass. For manure, 25% of N is added as  $\text{NH}_4^+$  and 75% as organic N with C:N ratio of 14. For hay, fertilization follows after a clipping and haying event.

Operation	Day of year	Fertilizer mass ( $\text{kg ha}^{-1}$ )	Fertilizer N-P-K
<b>Corn</b>			
Manure fertilizer	100	3500	03-01-00
Tillage moldboard	101		
Tillage disking	102		
Planting	121		
Fertilization	121	100	10-20-20
Fertilization	152	100	33-00-00
Harvest and kill crop			
<b>Soybean</b>			
Manure fertilizer	100	1875	03-01-00
Tillage disking	102		
Planting	121		
Harvest and kill			
<b>Oat for hay</b>			
Tillage chisel + cultivator	92		
Planting	97		
Fertilization	97	300	03-15-48
Fertilization	166	100	33-00-00
Harvest and kill	219		
<b>Hay (alfalfa + orchardgrass for hay)</b>			
Tillage (year 1)	101		
Planting (year 1)	105		
Fertilization manure (year 1)	100	3500	03-01-00
Fertilization (year 1)	259	100	02-11-45
Clipping and haying (4 times)	Various		
Fertilization all years (4 times)	Various	100	02-11-45
Kill (year 4)	303		

315 horizontal saturated macropore hydraulic conductivities, macropore depth, soil poros-  
316 ity, van Genuchten parameters, and canopy stomatal conductance. After calibration, land  
317 surface and hydrological states were spun up by recycling the meteorological forcing. Hy-  
318 drological states are considered steady when the change of watershed average ground-  
319 water storage is lower than 1 cm between the beginning and end of a simulation cycle.  
320 Steady state condition was reached in 32 years, which required recycling the meteorolo-  
321 gical forcing twice.

322 The land surface hydrological state variables after the spin-up were used to initial-  
323 ize the Cycles-L spin-up process. The Cycles-L model was run repeatedly by recycling  
324 the 16-year meteorological forcing and prescribed farm operations until the change of soil  
325 profile organic carbon was lower than  $0.01 \text{ Mg ha}^{-1}$ . Cycles-L reached steady state con-  
326 ditions after 11 simulation cycles, i.e., 167 simulation years.

327 We calibrated the crop model using the USDA-NASS survey corn yield by adjust-  
328 ing crop ecophysiological parameters that are site-dependent (rooting depth) and two  
329 related parameters that regulate growth potential, the radiation use efficiency (g of biomass  
330 accrued per MJ of radiation intercepted) and transpiration use efficiency (g of biomass  
331 accrued per kg of water transpired). The last two parameters were reduced to 2/3 of their  
332 default values, to represent in a simplified way limitations to growth not accounted for  
333 in the input data (shallower soils or compacted layers) or in the model (deficient root  
334 exploration due to rocks); the watershed soils can have locally high rock content (Saha  
335 et al., 2017). Overestimating yields can severely alter outputs mostly by increasing nu-  
336 trient extraction in harvested grain or forage.

337 Uncoupled Cycles simulations were performed to compare with Cycles-L outputs.  
338 The Cycles 1-D simulations used the most dominant soil type Calvin-Klinesville shaly  
339 silt loams (Ca), and the most prevailing crop rotation [corn (2 years)-soybean-corn-hay  
340 (4 years)]. As in Cycles-L, we ran four Cycles simulations, starting with different crops  
341 in the rotation, i.e., a corn (2 years)-soybean-corn-hay (4 years) simulation, a soybean-  
342 corn-hay (4 years)-corn (2 years) simulation, a hay (4 years)-corn (2 years)-soybean-corn  
343 simulation, and a hay (2 years)-corn (2 years)-soybean-corn-hay (2 years) simulation. Re-  
344 sults from the four simulations were averaged to be compared with Cycles-L.

## 345 4 Results

### 346 4.1 Simulation of stream discharge

347 Model simulation results from 2000 to 2015 after spin-up are presented below, and  
348 evaluated using field measurements or surveys.

349 Cycles-L captured the interannual variability of discharge, and accurately predicted  
350 the timing of most discharge events. The base flow rate predicted by Cycles-L compared  
351 well with observations. The Nash-Sutcliffe coefficient (NSE) of daily discharge for the  
352 entire simulation period was 0.55. The NSE, however, varied from year to year, and was  
353 as high as 0.85 in 2005. Discharge from multiple years was also averaged to each day of  
354 year to glean within-year patterns of measured and modeled discharge (Fig. 3b). The  
355 model captured the seasonal wet-dry cycles, and the predicted magnitude of discharge  
356 generally agreed well with observation. Cycles-L slightly overestimated discharge, ex-  
357 cept for late winter and spring. The NSE for the predicted multi-year average discharge  
358 was 0.68.

359 Flux-PIHM prediction was similar to Cycles-L (Fig. 3a) because both of them share  
360 the same hydrologic component but canopy cover is endogenous in Cycles-L and a forc-  
361 ing in Flux-PIHM. The NSE for Flux-PIHM daily discharge prediction was 0.60, which  
362 was slightly higher than Cycles-L (0.55). It should be noted that the land surface and  
363 hydrologic parameters in Cycles-L were calibrated by running Flux-PIHM, which may

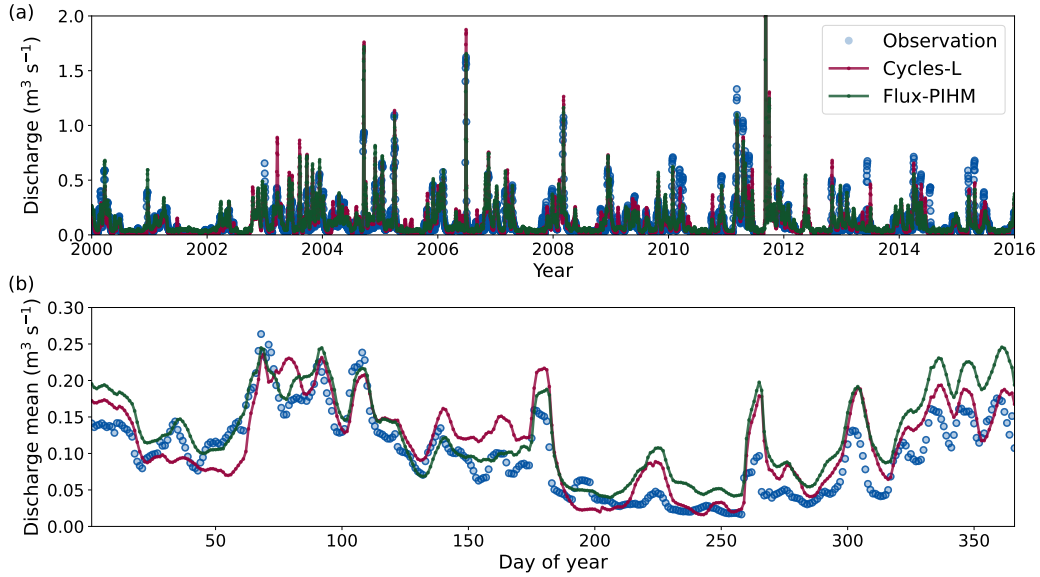


**Figure 3.** (a) Comparison of daily discharge between observations and outputs from Cycles-L and Flux-PIHM, from 1 Jan 2000 to 31 Dec 2015. (b) Comparison of daily discharge when averaged to each day of year.

364 cause Flux-PIHM to yield slightly better performance than Cycles-L. When averaged to  
 365 each day of year, Flux-PIHM also tended to overestimate discharge. Compared to Cy-  
 366 cles-L, Flux-PIHM produced higher predictions of discharge in spring, and lower predic-  
 367 tions in other seasons.

#### 368 4.2 Simulation of grain yield

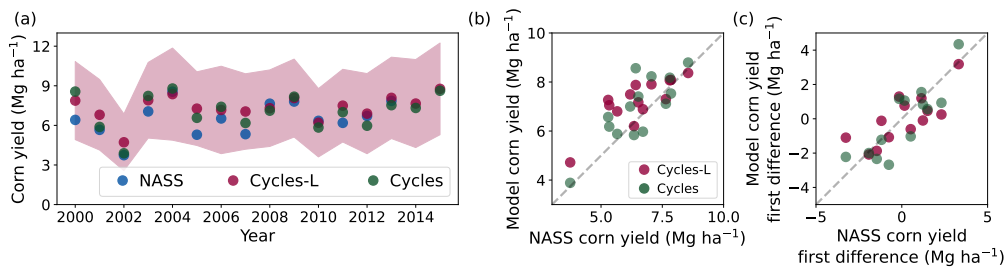


**Figure 4.** (a) Temporal variation of USDA-NASS survey corn yield and both Cycles-L and Cycles 1-D predicted annual average corn yield from 2000 to 2015. The USDA-NASS survey is for Northumberland County, PA. The shaded area represents the standard deviations of corn yield in space. (b) Cycles-L and Cycles 1-D predicted annual average corn yield versus USDA-NASS survey annual corn yield. (c) First difference of Cycles-L and Cycles 1-D predicted annual average corn yield versus first difference of USDA-NASS survey annual corn yield.

369 On average, both Cycles-L and Cycles captured the corn yield variation well (Fig. 4),  
 370 with  $R^2$  of 0.66 for Cycles-L and 0.65 for Cycles, and root mean square error (RMSE)  
 371 of 1.01 and 0.90  $\text{Mg ha}^{-1}$  for Cycles-L and Cycles, respectively. When comparing the

372 first differences of corn yield, which detrend yield increases with time due to technology,  
 373 the  $R^2$  for Cycles-L decreased to 0.58 and that for Cycles increased to 0.72. Cycles-L  
 374 tended to underestimate the interannual variability compared to Cycles (Fig. 4c). The  
 375 shaded area in Fig. 4(a) illustrates the spatial variation of corn grain yield predicted by  
 376 Cycles-L. The spatial variation of corn yield was larger when yield was higher, and smaller  
 377 when yield was lower. The standard deviations of corn yield in space varied between 2.2  
 378 and 3.5 Mg ha<sup>-1</sup>. The USDA-NASS survey reported yields were always within the pre-  
 379 dicted one-standard-deviation (Fig. 4a).

### 380 4.3 Simulation of mineral nitrogen discharge

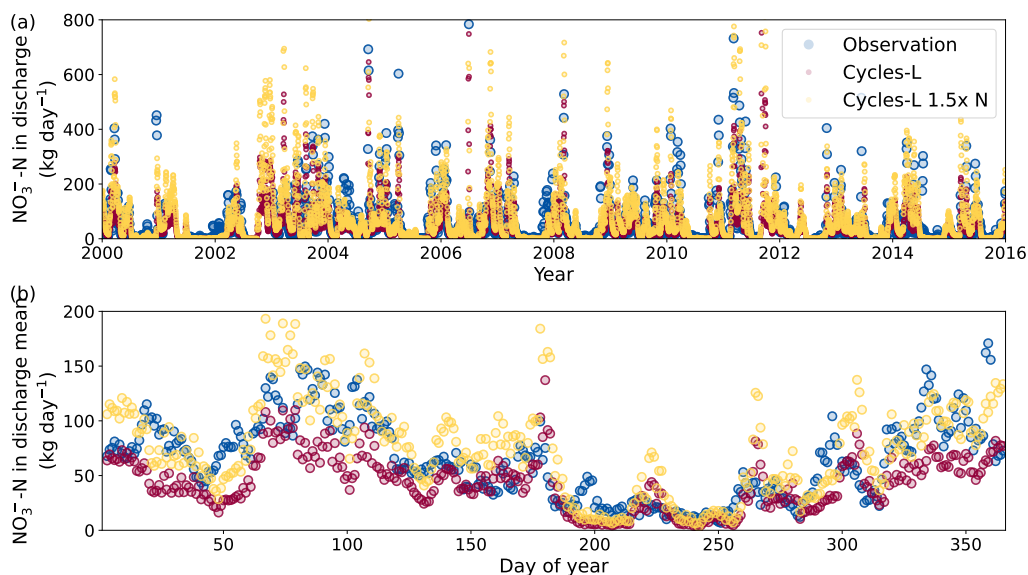


**Figure 5.** (a) Comparison of daily nitrate-N discharge between the observations and two Cycles-L simulations (1x N and 1.5x N), from 1 Jan 2000 to 31 Dec 2015. (b) Comparison of daily nitrate-N discharge when averaged to each day of year. When averaged to each day of year, a 3-day moving average was applied to both observations and predictions to better reveal the temporal patterns.

381 We focused on the N exported at the watershed outlet, where comparisons with  
 382 measurements allow a reality-bounded assessment of the impact of changing N fertiliza-  
 383 tion rates. The temporal patterns of water discharge (Fig. 3) and N discharge (Fig. 5)  
 384 are similar, because N discharge is controlled by water discharge. Accordingly, the N dis-  
 385 charge pattern was correctly simulated by Cycles-L with an NSE of 0.58, but the N mass  
 386 discharged through the stream was consistently underestimated compared with measure-  
 387 ments (Fig. 5). The observed and predicted average NO<sub>3</sub><sup>-</sup>-N discharge were 63.8 and 46.1 kg day<sup>-1</sup>.

### 388 4.4 Simulation of mineral nitrogen concentration in the stream

389 Because the stream discharge was slightly overestimated and NO<sub>3</sub><sup>-</sup>-N underestimated,  
 390 the concentration of NO<sub>3</sub><sup>-</sup>-N was also underestimated, as was the seasonal variation in  
 391 NO<sub>3</sub><sup>-</sup>-N concentration (Fig. 6). The average observed NO<sub>3</sub><sup>-</sup>-N concentration in the stream  
 392 was 5.4 mg L<sup>-1</sup>, with a pronounced W-shaped seasonal pattern with highs in early sum-  
 393 mer and in winter, and lows in spring and autumn (Fig. 6b). Interannual variability was  
 394 also noticeable. The simulations consistently underestimated the concentration of NO<sub>3</sub><sup>-</sup>-N,

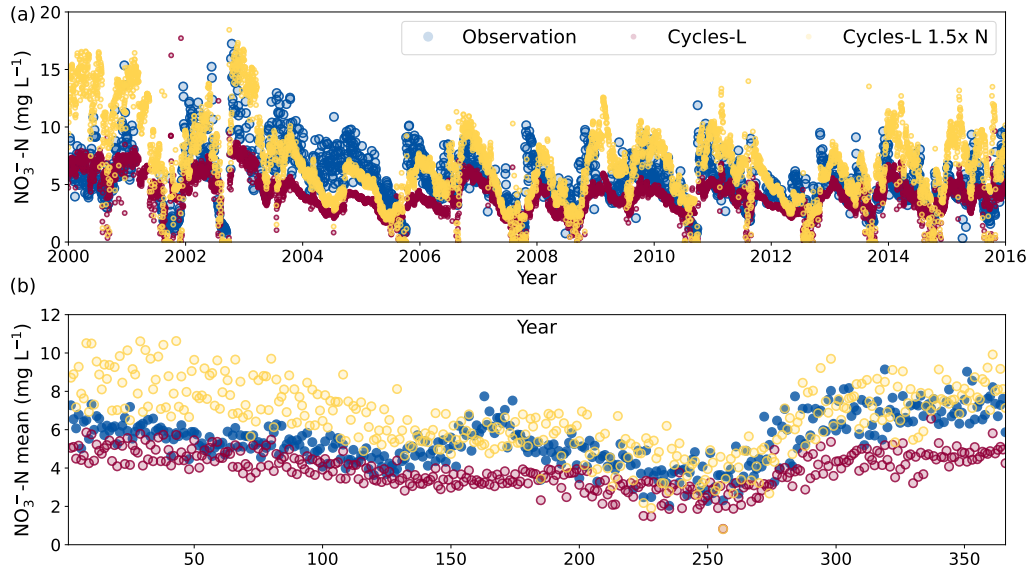


**Figure 6.** (a) Comparison of daily stream nitrate-N concentrations between observations and two Cycles-L simulations (1x N and 1.5x N), from 1 Jan 2000 to 31 Dec 2015. (b) Comparison of daily nitrate-N concentrations when averaged to each day of year.

395 on average by about 30%, and significantly underestimated the magnitude of seasonal  
 396 variations.

#### 397 4.5 Spatial pattern of simulated nitrogen fluxes

**Table 2.** Simulated and observed nitrogen fluxes. All fluxes are watershed annual average.

N flux	Cycles-L	Cycles-L 1.25xN	Cycles-L 1.5xN	Observed
	(kg ha <sup>-1</sup> yr <sup>-1</sup> )			
Fixation and deposition	45.0	41.9	38.7	N/A
Fertilization (manure)	54.8	68.4	82.2	N/A
Fertilization (synthetic)	30.2	37.8	45.3	N/A
Volatilization	9.4	10.6	11.8	N/A
Denitrification	8.4	10.7	13.3	N/A
N <sub>2</sub> O emission from nitrification	0.5	0.6	0.7	N/A
N in Harvest	77.3	83.7	89.1	N/A
N in discharge	22.7	29.9	38.8	31.4

398 Since the model has been run to steady state, the change of N storage in the sys-  
 399 tem was low. On average, most N removals other than discharge occurred through N har-  
 400 vest, NH<sub>3</sub>-N volatilization, and NO<sub>3</sub><sup>-</sup>-N denitrification (Table 2).

401 Due to the distribution of the cropland and forestland, N inputs had a marked spa-  
 402 tial distribution (Fig. 7). Yet, the spatial patterns of N losses were also shaped by to-  
 403 pography and soils that alter hydrology. The spatial pattern of N input was clearly con-  
 404 trolled by crop management. Forests and the areas with the hay rotation have low N in-

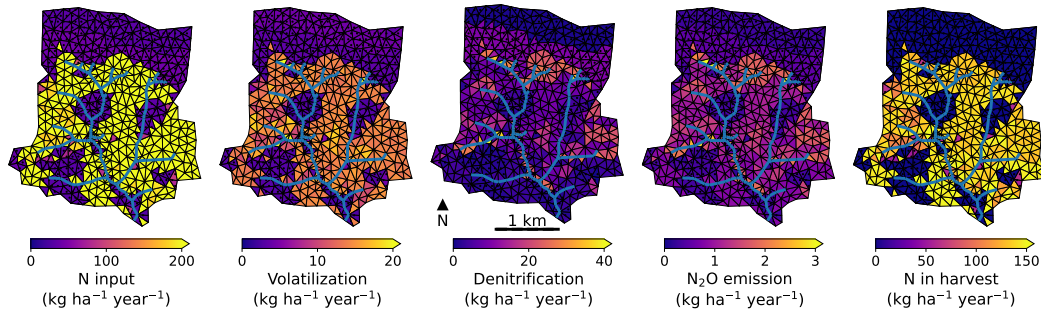


**Figure 7.** Spatial patterns of nitrogen fluxes (nitrogen input, nitrogen volatilization, denitrification,  $\text{N}_2\text{O}$  emission, and nitrogen in harvest) as predicted by Cycles-L. For each model grid, the fluxes were averaged over the whole simulation period. The dotted areas represent the forests and areas with the hay rotation. The blue lines represent river segments.

405 put because there was no fertilization but only deposition and biological fixation. The  
 406 spatial pattern of  $\text{NH}_3\text{-N}$  volatilization was highly correlated with the pattern of fertiliza-  
 407 tion. The spatial patterns of denitrification and  $\text{N}_2\text{O}$  emission demonstrate the complex  
 408 interactions between crop management and topography. The forests had a lower deni-  
 409 trification rate (and  $\text{N}_2\text{O}$  emission) compared to areas with crop rotations. For the ar-  
 410 eas with crop rotations, denitrification rates (and  $\text{N}_2\text{O}$  emission) were higher in head-  
 411 waters and some regions of convergent flow or flat terrain near the stream (but not all),  
 412 where soil water content was higher. Nitrogen harvest was largest in areas with a high  
 413 frequency of corn and soybean.

## 414 5 Discussion

### 415 5.1 Simulating hydrology

416 Cycles-L captured the interannual variability of discharge, and accurately predicted  
 417 the timing of peak discharge events and base flow rates with minimum manual calibra-  
 418 tion. This is in line with the high fidelity of the PIHM family models demonstrated for  
 419 multiple watersheds (Shi et al., 2013, 2015; Jepsen et al., 2016; Crow et al., 2018; Zhang  
 420 et al., 2018; Xiao et al., 2019; Zheng et al., 2021). Among the desirable future improve-  
 421 ments are to represent explicitly perched water movement on top of Bt horizons, which  
 422 would allow lateral water transport overlaying unsaturated soil layers. Currently, this  
 423 process is lumped in the lateral flow calibration parameters. While modeling it explic-  
 424 itly may not improve the overall accuracy of discharge predictions, it may affect min-  
 425 eral N (and other constituents) transport. Similar considerations apply to modeling wa-  
 426 ter flux through tile drains, with the practical caveat that the location of tile drains is  
 427 often unknown. When the tile drain network is well mapped it can be explicitly simu-  
 428 lated although at the cost of a very dense grid (De Schepper et al., 2015). Nonetheless,  
 429 while the model performs well in its current formulation, future developments should in-  
 430 clude an explicit representation of tile drains as submerged channels that interact with  
 431 groundwater.

432 Compared with other spatially distributed agroecosystem hydrological systems, which  
 433 usually have rigid rectangular model grids, the unstructured triangular grids of Cycles-L  
 434 provides both computational efficiency and optimal representations of local heterogene-  
 435 ity. Unstructured triangular grids capture with ease watershed boundaries, stream net-  
 436 works, and soil and vegetation units (Qu & Duffy, 2007; Kumar et al., 2010; De Schep-  
 437 per et al., 2015). Because grid sizes can differ in Cycles-L, coarser grids can be used in

438 locations with simple topography and low land surface heterogeneity to improve model  
 439 efficiency, while finer grids can be used to capture complex topography and spatial het-  
 440 erogeneity in soil and vegetation, an approach that is already suggested by the unstruc-  
 441 tured mesh used to represent tile drains by De Schepper et al. (2015). These features  
 442 enable applications for precision agriculture in a cohesive framework. Cycles-L’s unique  
 443 capability to simulate the two-way interaction between stream and riparian zones makes  
 444 it extremely useful to evaluate interventions in agricultural areas along floodplains where  
 445 flooding damage risk is high (Collins et al., 2022).

## 446 5.2 Simulating nitrogen discharge and concentration

447 When using the fertilization rate as prescribed by the survey data (Hirt et al., 2020),  
 448 the model prediction of water discharge and corn yield agreed well with the observations  
 449 and survey (Figures 3 and 4), but underestimated the stream  $\text{NO}_3^-$ -N concentration and  
 450  $\text{NO}_3^-$ -N discharge (Figures 5 and 6). The discharge underestimation amounted to  $9.7 \text{ kg ha}^{-1} \text{ y}^{-1}$   
 451 of N (Table 2). Among the possible reasons are that the model is overestimating other  
 452 N losses or that N inputs are underreported. Therefore, we ran exploratory Cycles-L sim-  
 453 ulations with arbitrary N input increases of 25% (not shown in the figures) and 50% over  
 454 the survey data (hereafter, Cycles-L 1.25x N and Cycles-L 1.5x N simulations).

455 The  $\text{NO}_3^-$ -N in discharge predicted by the Cycles-L 1.5x N simulation was higher  
 456 than the observed discharge (+7.4 over the observed  $31.4 \text{ kg NO}_3^- \text{-N ha}^{-1} \text{ y}^{-1}$ ) but closer  
 457 to that in the default simulation; the  $\text{NO}_3^-$ -N in discharge predicted with Cycles-L 1.25x N  
 458 almost matched the observed discharge (Table 2). Although the 1.5x N simulation over-  
 459 estimated stream  $\text{NO}_3^-$ -N concentration in winter and spring, deviations in multi-year  
 460 average N discharge for this time period were small, because the model’s underestima-  
 461 tion of water discharge for the same time period (Fig. 3b) compensated for deviations  
 462 in  $\text{NO}_3^-$ -N concentration. The 1.5x N simulation substantially overestimated  $\text{NO}_3^-$ -N con-  
 463 centration in 2000 and 2001 and underestimated it in 2003 and 2004 (Fig. 6). For other  
 464 years, the predicted  $\text{NO}_3^-$ -N concentration agreed well with observations, especially for  
 465 the second half of the simulation (from 2008 to 2016), despite missing some peaks. When  
 466 averaged to each day of year, the model captured the seasonal variation of  $\text{NO}_3^-$ -N con-  
 467 centration change, but overestimated the concentration in late winter and early spring  
 468 (Fig. 6b).

469 The Cycles-L 1x N, 1.25x N, and 1.5x N simulations produced almost identical corn  
 470 yield and water discharge. It suggests that crop growth was not N limited in WE-38 even  
 471 when using the 1x fertilization rate. Because crop growth was similar between the two  
 472 simulations, evapotranspiration simulations were close as well, hydrology was not affected,  
 473 and the three simulations produced similar stream discharge. Adding more N fertilizer,  
 474 however, increased stream N concentration. It should be noted that adding 50% more  
 475 N fertilizer did not increase N inputs to the watershed proportionally because of a par-  
 476 allel reduction in N biological fixation of  $6.3 \text{ kg ha}^{-1} \text{ y}^{-1}$  of N (Table 2). If we were to  
 477 assume that indeed, inputs of N were underestimated, and that they would scale linearly  
 478 between our 1x and 1.5x simulations, we estimate that N inputs obtained through sur-  
 479 veys were underestimated by 25 to 30%.

480 As in Ator and Garcia (2016), denitrification was a significant loss pathway. When  
 481 spatially averaged over the whole simulation period (from 2000 to 2015), denitrification  
 482 rates generally increased as N input increased within each crop rotation type (Fig. 8),  
 483 but strong variation existed depending on the rotation and field location. There seems  
 484 to be a correlation between well drained locations and the location of corn and soybean  
 485 in the field (Fig. 2), likely reflecting producers’ choices that facilitate field operations in  
 486 cash crops, which may result in lesser than expected N denitrification losses in those fields  
 487 (Fig. 8). However,  $\text{NO}_3^-$ -N is transported mostly through groundwater, and grids that  
 488 gain  $\text{NO}_3^-$ -N through leaching from other grids may have higher denitrification rates than

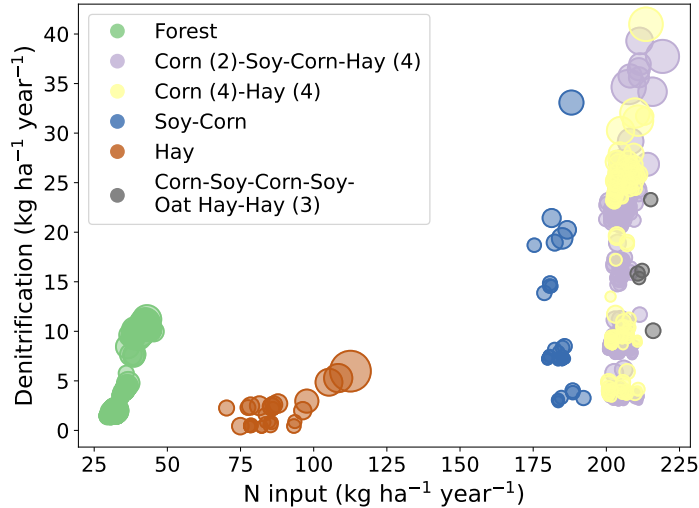


**Figure 8.** Average denitrification rate vs average nitrogen input as predicted by Cycles-L. Each circle represents one model grid, averaged over the whole simulation period. The sizes of the circles represent the degrees of soil saturation. Different colors represent different land uses/crop rotations.

489 those expected based only on surface N input. While forests and hay fields have lower  
 490 N input than the other crop rotations, most cropping model grids have average N input  
 491 between 175 and 225 kg ha<sup>-1</sup> y<sup>-1</sup>, but their simulated denitrification rates varied sig-  
 492 nificantly, from around 5 to 40 kg NO<sub>3</sub><sup>-</sup>-N ha<sup>-1</sup> y<sup>-1</sup>, in large part due to hydrological  
 493 control of leaching and denitrification. The movement of water alters both NO<sub>3</sub><sup>-</sup>-N and  
 494 oxygen availability in space, which leads to significantly different spatial denitrification  
 495 rates (Groffman et al., 2009). Within each crop rotation type, denitrification rates tend  
 496 to increase when soil wetness increases (represented by the circles' size in Fig. 8), which  
 497 reflects the dominant control of oxygen on denitrification rates in the model (i.e., air filled  
 498 pore space decreases and so does oxygen replenishment). The importance of represent-  
 499 ing these spatial interactions to model hot spots and hot moments of denitrification has  
 500 been highlighted earlier by Groffman et al. (2009) and measured in the field by Saha et  
 501 al. (2017). Our modeling framework advances in that direction. Improvements are needed  
 502 to represent denitrification in stream sediments and to include physical features such as  
 503 the specific location of buried carbon sources (Hill et al., 2014), to further refine our un-  
 504 derstanding and modeling of denitrification spatial distribution (Wallace et al., 2020).

### 505 **5.3 Strength of Cycles-L and opportunities for improvement**

506 Because of its spatially distributed nature, Cycles-L represents a step forward to  
 507 simulate landscape level processes such as groundwater and stream water transport of  
 508 reactive N and other compounds as affected by crop rotation, soil type, and weather vari-  
 509 ations within the watershed domain. It can also represent the heterogeneity of agro-  
 510 ecosystem processes caused by topography, soil heterogeneity, and management practices,  
 511 owing to its physically-based hydrologic component and ability to simulate horizontal  
 512 and vertical transport of mineral N with water. By extension, other nutrients like sol-  
 513 uble phosphorus (McConnell et al., 2020), dissolved organic C (Pabich et al., 2001), and  
 514 agrochemicals (Hladik & Kolpin, 2015) can be integrated in the same framework.

515 Cycles-L can be an important tool to evaluate costly interventions *in silico* before  
516 deployment in the field, as complex interactions among subsurface, land surface, and crops  
517 can be explored before committing resources on the ground, as exemplified by a com-  
518 parable model using a square grid domain (Beaujouan et al., 2001). Similarly, Cycles-L  
519 can become a powerful tool for precision agriculture and precision conservation, becom-  
520 ing a core component of artificial intelligence applications (Gil et al., 2021). The spa-  
521 tial and temporal richness of the model outputs coupled with immersive visuals open new  
522 opportunities to represent the dynamics of agroecosystems to develop research, educa-  
523 tional, and public engagement tools (C. Wang et al., 2019).

524 Comparing Cycles 1-D average corn yield with county-level yield averages, a coarse  
525 comparison due to the amalgamation of disparate scales, indicates that overall Cycles  
526 correctly captures the effect of interannual variations in weather on crop yield. So do other  
527 1-D cropping system models applied in the region (Castaño-Sánchez et al., 2020). Cy-  
528 cles-L did not improve upon these results, although the comparison scope is limited to  
529 this small watershed. The simulations with Cycles-L increased the minimum yield most  
530 likely due to redistribution of subsurface water in drier years. It remains to be tested if  
531 an even finer resolution (smaller triangles) would render a better representation of hy-  
532 drology and crop growth and yield. Such finer resolution would also require using dense,  
533 grid-specific soil input information. While such soil information might not be available,  
534 yield maps that would allow such testing are already regularly available, and assessing  
535 the effect of a finer resolution in representing certain processes is needed to advance ap-  
536 plications in precision agriculture.

537 Macropore flow in Flux-PIHM lumps vertical bypass flow, but also fast lateral flow  
538 of perched water that reaches the stream with lesser mixing with water in the non-saturated  
539 soil matrix. In this watershed, measurements have revealed that water can reach streams  
540 through ephemeral springs that exfiltrate after lateral transport (Redder et al., 2021),  
541 and that water can have high concentration of  $\text{NO}_3^-$ -N that reflects limited mixing with  
542 groundwater (M. R. Williams et al., 2015). When measuring in-stream  $\text{NO}_3^-$ -N concen-  
543 tration, this spring contribution of water and  $\text{NO}_3^-$ -N can cause spikier readings in stream  
544  $\text{NO}_3^-$ -N concentration than when water reaching the stream is mixed with groundwa-  
545 ter, and is the case for Flux-PIHM (except for direct runoff). This is clearly difficult to  
546 represent with lumped parameters, which can help explain the subdued variation in the  
547 modeled versus measured  $\text{NO}_3^-$ -N concentration in the stream (Fig. 6).

548 The quality of Cycles-L predictions depends on both model structure and input data  
549 quality. To represent, for example, large N discharge events, accurate input of the amount,  
550 timing, and composition of the N amendments is critical. However, the composition of  
551 animal manure is highly variable (Griffin et al., 2005), so that there is an inherent vari-  
552 ance in the addition of N and other nutrients to fields or watersheds via manure. In this  
553 study, manure N input represented 42% of the N input in the 1x N scenario (Table 2),  
554 and was on average twice as large as the  $\text{NO}_3^-$ -N watershed discharge. In addition, for  
555 the simulations presented here, the prescribed management practices have the same plant-  
556 ing dates, tillage dates and practices, and fertilization dates and rates every year, which  
557 are approximately correct on average but likely incorrect in any given year of the 16-year  
558 simulation period. Therefore using the surveyed management data introduces uncertainty  
559 that would reflect in deviations of stream flow and especially  $\text{NO}_3^-$ -N concentration (Fig. 6)  
560 independently of the model algorithms. The underestimation of  $\text{NO}_3^-$ -N discharge when  
561 using survey data to represent fertilizer inputs (1x) and the improvement through the  
562 modeled 1.25x and 1.5x scenarios suggest that N inputs through fertilizer could have been  
563 underestimated on average by 30%. Indeed, a mismatch between field survey data on  
564 N (and phosphorus) input and that needed to match crop yield and other variables has  
565 been reported before (USDA-NRCS, 2012, page 30).

566 Cycles-L couples a hydrologic model (PIHM), land surface model (Noah LSM), and  
567 agroecosystem model (Cycles) together. The interactions among these components are

568 complex and the number of parameters involved is large even when using a conservative  
 569 approach for model development. Parameter sensitivity in Flux-PIHM has been exam-  
 570 ined in previous studies (Shi et al., 2014; Xiao et al., 2019), which revealed complex in-  
 571 teractions among model parameters and between land surface-subsurface processes that  
 572 are inherited in Cycles-L. Sensitivity analysis of Cycles-L can help identify critical model  
 573 parameterization and reveal any potential dependence of model results on grid resolu-  
 574 tion.

575 Operationally, it is simple to set up and run 1-D models like a stand alone Cycles  
 576 1-D with standardized inputs. Once the soil profile and weather forcing are formatted  
 577 to conform to requirements, there is no impediment to run the model. Setting up and  
 578 running 3-D models is less straightforward. While the generation of input files, grid and  
 579 stream network has been automated in the past for CONUS to provide users a starting  
 580 point at the HUC12 level (Leonard & Duffy, 2014), automation does not warrant that  
 581 the setup provides a stable frame to represent hydrology. Often, the grid and stream net-  
 582 work setup needs to be streamlined to secure convergence of fluxes and state variables  
 583 or to avoid resorting to small time steps that slow down execution. However, once a set  
 584 up is ready, it can be stored, shared, and re-used efficiently, and support running new  
 585 scenarios or applications that need to combine measurements and modeling (e.g., Drake  
 586 et al., 2018) with agility.

## 587 6 Conclusions

588 Cycles-L is among the first next generation physically-based spatially-distributed  
 589 agroecosystem models that can represent landscape processes. The coupling of biogeo-  
 590 chemical and hydrologic processes at the catchment scale places this model between 1-D  
 591 models that simplify terrain and other attributes, and global models that connect at-  
 592 mospheric volumes in 3-D but are underlined by simplified land models. Cycles-L oc-  
 593 cupies therefore a unique operational space relevant to simulate interventions in the land-  
 594 scape.

595 In the test case presented here for Central Pennsylvania, Cycles-L simulated well  
 596 hydrology, grain crops yield, and N exports in the stream, despite some uncertainty in  
 597 the quality of the input data. Cycles-L retains, therefore, the strengths of Flux-PIHM  
 598 (Shi et al., 2013) and the 1-D Cycles model (Kemanian et al., 2022). Compared to the  
 599 uncoupled Flux-PIHM (water discharge) and Cycles (crop yield) models, the predictions  
 600 of Cycles-L are as good if not improved. The model skill at predicting the impact of to-  
 601 pography, soil heterogeneity, and crop management on N fluxes temporally and spatially  
 602 can expand the domain of *in silico* agroecosystem analysis to landscape levels.

603 Further progress will depend on continuously balancing the complexity of the model  
 604 algorithms with concomitant improvements in input quality, to take advantage of increas-  
 605 ing computing capacity and to represent landscapes with increasing fidelity. We envi-  
 606 sion that tools like Cycles-L will become a critical component of the analytical toolkit  
 607 of both academic and non-academic communities.

## 608 Acknowledgments

609 Funding for this research provided by DoE BETO grant DE-EE0007088/0000, EPA Grant  
 610 RD835568, NSF-CNHS grant ICER-1517823, and USDA-NIFA Award 2012-68005-19703  
 611 and 2020-68012-31824, and the College of Agricultural Sciences at Penn State via USA  
 612 Hatch Appropriations under Project PEN04571 and Accession 1003346. The NLDAS-2  
 613 data used in this study were acquired as part of the mission of NASA’s Earth Science  
 614 Division and archived and distributed by the Goddard Earth Sciences (GES) Data and  
 615 Information Services Center (DISC).

## References

616

- 617 Arnold, J. G., Srinivasan, R., Muttiah, R. S., & Williams, J. R. (1998). Large area  
618 hydrologic modeling and assessment. Part I: Model development. *JAWRA*  
619 *Journal of the American Water Resources Association*, *34*(1), 73–89. doi:  
620 10.1111/j.1752-1688.1998.tb05961.x
- 621 Ator, S. W., & Garcia, A. M. (2016). Application of SPARROW Modeling to un-  
622 derstanding contaminant fate and transport from uplands to streams. *Journal*  
623 *of the American Water Resources Association (JAWRA)*, *52*(3), 685–704. doi:  
624 10.1111/1752-1688.12419
- 625 Baker, J. M., Ochsner, T. E., Venterea, R. T., & Griffis, T. J. (2007). Tillage and  
626 soil carbon sequestration—What do we really know? *Agriculture, Ecosystems*  
627 *& Environment*, *118*(1), 1–5. doi: 10.1016/j.agee.2006.05.014
- 628 Bao, C., Li, L., Shi, Y., & Duffy, C. (2017). Understanding watershed hydrogeo-  
629 chemistry: 1. Development of RT-Flux-PIHM. *Water Resources Research*,  
630 *53*(3), 2328–2345. doi: 10.1002/2016WR018934
- 631 Basso, B., Bertocco, M., Sartori, L., & Martin, E. C. (2007). Analyzing the effects  
632 of climate variability on spatial pattern of yield in a maize–wheat–soybean  
633 rotation. *European Journal of Agronomy*, *26*(2), 82–91. doi: 10.1016/  
634 j.eja.2006.08.008
- 635 Batchelor, W. D., Basso, B., & Paz, J. O. (2002). Examples of strategies to analyze  
636 spatial and temporal yield variability using crop models. *European Journal of*  
637 *Agronomy*, *18*(1), 141–158. doi: 10.1016/S1161-0301(02)00101-6
- 638 Beaujouan, V., Durand, P., & Ruiz, L. (2001). Modelling the effect of the spatial  
639 distribution of agricultural practices on nitrogen fluxes in rural catchments.  
640 *Ecological Modelling*, *137*(1), 93–105. doi: 10.1016/S0304-3800(00)00435-X
- 641 Bhatt, G., Kumar, M., & Duffy, C. J. (2014). A tightly coupled GIS and distributed  
642 hydrologic modeling framework. *Environmental Modelling & Software*, *62*, 70–  
643 84. doi: 10.1016/j.envsoft.2014.08.003
- 644 Bonilla, C. A., Norman, J. M., & Molling, C. C. (2007). Water erosion estimation  
645 in topographically complex landscapes: Model description and first verifi-  
646 cations. *Soil Science Society of America Journal*, *71*(5), 1524–1537. doi:  
647 10.2136/sssaj2006.0302
- 648 Bonilla, C. A., Norman, J. M., Molling, C. C., Karthikeyan, K. G., & Miller, P. S.  
649 (2008). Testing a grid-based soil erosion model across topographically complex  
650 landscapes. *Soil Science Society of America Journal*, *72*(6), 1745–1755. doi:  
651 10.2136/sssaj2007.0310
- 652 Booker, J. D., Lascano, R. J., Evett, S. R., & Zartman, R. E. (2014). Evaluation  
653 of a landscape-scale approach to cotton modeling. *Agronomy Journal*, *106*(6),  
654 2263–2279. doi: 10.2134/agronj14.0202
- 655 Booker, J. D., Lascano, R. J., Molling, C. C., Zartman, R. E., & Acosta-Martínez,  
656 V. (2015). Temporal and spatial simulation of production-scale ir-  
657 rigated cotton systems. *Precision Agriculture*, *16*(6), 630–653. doi:  
658 10.1007/s11119-015-9397-6
- 659 Boote, K. J., Jones, J. W., Hoogenboom, G., & White, J. W. (2010). The role of  
660 crop systems simulation in agriculture and environment. *International Journal*  
661 *of Agricultural and Environmental Information Systems (IJAEIS)*, *1*(1), 41–54.  
662 doi: 10.4018/jaeis.2010101303
- 663 Bryant, R. B., Veith, T. L., Feyereisen, G. W., Buda, A. R., Church, C. D., Folmar,  
664 G. J., . . . Kleinman, P. J. A. (2011). U.S. Department of Agriculture Agri-  
665 cultural Research Service Mahantango Creek Watershed, Pennsylvania, United  
666 States: Physiography and history. *Water Resources Research*, *47*, W08701.  
667 doi: 10.1029/2010WR010056
- 668 Buda, A. R., Feyereisen, G. W., Veith, T. L., Folmar, G. J., Bryant, R. B., Church,  
669 C. D., . . . Kleinman, P. J. A. (2011). U.S. Department of Agriculture Agri-  
670 cultural Research Service Mahantango Creek Watershed, Pennsylvania, United

- 671 States: Long-term stream discharge database. *Water Resources Research*,  
672 47(8). doi: 10.1029/2010WR010059
- 673 Campbell, G. S. (1985). *Soil physics with BASIC: transport models for soil-plant*  
674 *systems*. Amsterdam: Elsevier.
- 675 Castaño-Sánchez, J. P., Rotz, C. A., Karsten, H. D., & Kemanian, A. R. (2020).  
676 Elevated atmospheric carbon dioxide effects on maize and alfalfa in the North-  
677 east US: A comparison of model predictions and observed data. *Agricultural*  
678 *and Forest Meteorology*, 291, 108093. doi: 10.1016/j.agrformet.2020.108093
- 679 Chen, E., & Mackay, D. (2004). Effects of distribution-based parameter aggregation  
680 on a spatially distributed agricultural nonpoint source pollution model. *Jour-*  
681 *nal of Hydrology*, 295(1), 211–224. doi: 10.1016/j.jhydrol.2004.03.029
- 682 Chen, F., & Dudhia, J. (2001). Coupling an advanced land surface–hydrology  
683 model with the Penn State–NCAR MM5 modeling system. Part I: Model im-  
684 plementation and sensitivity. *Monthly Weather Review*, 129(4), 569–585. doi:  
685 10.1175/1520-0493(2001)129<0569:CAALSH>2.0.CO;2
- 686 Church, C. D., Veith, T. L., Folmar, G. J., Buda, A. R., Feyereisen, G. W., Bryant,  
687 R. B., . . . Kleinman, P. J. A. (2011). U.S. Department of Agriculture Agri-  
688 cultural Research Service Mahantango Creek Watershed, Pennsylvania, United  
689 States: Long-term water quality database. *Water Resources Research*, 47(8),  
690 W08704. doi: 10.1029/2010WR010060
- 691 Collins, E. L., Sanchez, G. M., Terando, A., Stillwell, C. C., Mitasova, H., Sebas-  
692 tian, A., & Meentemeyer, R. K. (2022). Predicting flood damage probability  
693 across the conterminous United States. *Environmental Research Letters*, 17(3),  
694 034006. doi: 10.1088/1748-9326/ac4f0f
- 695 Confalonieri, R., Orlando, F., Paleari, L., Stella, T., Gilardelli, C., Movedi, E.,  
696 . . . Acutis, M. (2016). Uncertainty in crop model predictions: What is  
697 the role of users? *Environmental Modelling & Software*, 81, 165–173. doi:  
698 10.1016/j.envsoft.2016.04.009
- 699 Cowan, I. R. (1978). Stomatal behaviour and environment. In R. D. Preston &  
700 H. W. Woolhouse (Eds.), (Vol. 4, pp. 117–228). Academic Press. doi: 10.1016/  
701 S0065-2296(08)60370-5
- 702 Cowan, I. R. (1982). Regulation of water use in relation to carbon gain in  
703 higher plants. In O. L. Lange, P. S. Nobel, C. B. Osmond, & H. Ziegler  
704 (Eds.), *Physiological plant ecology ii: Water relations and carbon assimila-*  
705 *tion* (pp. 589–613). Berlin, Heidelberg: Springer Berlin Heidelberg. doi:  
706 10.1007/978-3-642-68150-9\_18
- 707 Crow, W. T., Milak, S., Moghaddam, M., Tabatabaeenejad, A., Member, S.,  
708 Jaruwatanadilok, S., . . . Cuenca, R. H. (2018). Spatial and Temporal  
709 Variability of Root-Zone Soil Moisture Acquired From Hydrologic Mod-  
710 eling and AirMOSS P -Band Radar. *IEEE Journal of Selected Topics*  
711 *in Applied Earth Observations and Remote Sensing*, PP(12), 1–13. doi:  
712 10.1109/JSTARS.2018.2865251
- 713 De Schepper, G., Therrien, R., Refsgaard, J. C., & Hansen, A. L. (2015). Simulating  
714 coupled surface and subsurface water flow in a tile-drained agricultural catch-  
715 ment. *Journal of Hydrology*, 521, 374–388. doi: 10.1016/j.jhydrol.2014.12.035
- 716 de Saint-Venant, B. (1871). Theory of unsteady water flow with application to floods  
717 and to propagation of tides in river channels. *Proceedings of French Academy*  
718 *of Science*, 73, 148–154.
- 719 Drake, C. W., Jones, C. S., Schilling, K. E., Amado, A. A., & Weber, L. J. (2018).  
720 Estimating nitrate-nitrogen retention in a large constructed wetland using  
721 high-frequency, continuous monitoring and hydrologic modeling. *Ecological*  
722 *Engineering*, 117, 69–83. doi: 10.1016/j.ecoleng.2018.03.014
- 723 Ek, M. B., Mitchell, K. E., Lin, Y., Rogers, E., Grunmann, P., Koren, V., . . .  
724 Tarpley, J. D. (2003). Implementation of Noah land surface model ad-  
725 vances in the National Centers for Environmental Prediction operational

- mesoscale Eta model. *Journal of Geophysical Research*, 108(D22), 8851.  
doi: 10.1029/2002JD003296
- Foley, J. A., Prentice, I. C., Ramankutty, N., Levis, S., Pollard, D., Sitch, S., & Haxeltine, A. (1996). An integrated biosphere model of land surface processes, terrestrial carbon balance, and vegetation dynamics. *Global Biogeochemical Cycles*, 10(4), 603–628. doi: 10.1029/96GB02692
- Francesconi, W., Smith, D. R., Heathman, G. C., Wang, X., & Williams, C. O. (2014). Monitoring and APEX Modeling of no-till and reduced-till in tile-drained agricultural landscapes for water quality. *Transactions of the American Society of Agricultural and Biological Engineers*, 57(3), 777–789. doi: 10.13031/trans.57.10332
- Frank, S., Fürst, C., Koschke, L., & Makeschin, F. (2012). A contribution towards a transfer of the ecosystem service concept to landscape planning using landscape metrics. *Ecological Indicators*, 21, 30–38. doi: 10.1016/j.ecolind.2011.04.027
- Gassman, P. W., Williams, J. R., Wang, X., Saleh, A., Osei, E., Hauck, L. M., . . . Flowers, D. J. (2010). The Agricultural Policy/Environmental eXtender (APEX) Model: An emerging tool for landscape and watershed environmental analyses. *Transactions of the American Society of Agricultural and Biological Engineers*, 53(3), 711–740. doi: 10.13031/2013.30078
- Gil, Y., Garijo, D., Khider, D., Knoblock, C. A., Ratnakar, V., Osorio, M., . . . Shu, L. (2021). Artificial intelligence for modeling complex systems: Taming the complexity of expert models to improve decision making. *ACM Trans. Interact. Intell. Syst.*, 11(2). doi: 10.1145/3453172
- Griffin, T. S., He, Z., & Honeycutt, C. W. (2005). Manure composition affects net transformation of nitrogen from dairy manures. *Plant and Soil*, 273(1), 29–38. doi: 10.1007/s11104-004-6473-5
- Groffman, P. M., Butterbach-Bahl, K., Fulweiler, R. W., Gold, A. J., Morse, J. L., Stander, E. K., . . . Vidon, P. (2009). Challenges to incorporating spatially and temporally explicit phenomena (hotspots and hot moments) in denitrification models. *Biogeochemistry*, 93(1), 49–77. doi: 10.1007/s10533-008-9277-5
- Hill, A. R., Devito, K. J., & Vidon, P. G. (2014). Long-term nitrate removal in a stream riparian zone. *Biogeochemistry*, 121(2), 425–439. doi: 10.1007/s10533-014-0010-2
- Hindmarsh, A. C., Brown, P. N., Grant, K. E., Lee, S. L., Serban, R., Shumaker, D. E., & Woodward, C. S. (2005). SUNDIALS: Suite of nonlinear and differential/algebraic equation solvers. *ACM Transactions on Mathematical Software*, 31(3), 363–396.
- Hirt, C. C., Veith, T. L., Collick, A. S., Yetter, S. E., & Brooks, R. P. (2020). Headwater stream condition and nutrient runoff: Relating SWAT to empirical ecological measures in an agricultural watershed in Pennsylvania. *Journal of Environmental Quality*, 49(3), 557–568. doi: 10.1002/jeq2.20032
- Hladik, M. L., & Kolpin, D. W. (2015). First national-scale reconnaissance of neonicotinoid insecticides in streams across the USA. *Environmental Chemistry*, 13(1), 12–20. doi: 10.1071/EN15061
- Jacob, D., Petersen, J., Eggert, B., Alias, A., Christensen, O. B., Bouwer, L. M., . . . Yiou, P. (2014). EURO-CORDEX: New high-resolution climate change projections for European impact research. *Regional Environmental Change*, 14(2), 563–578. doi: 10.1007/s10113-013-0499-2
- Jepsen, S. M., Harmon, T. C., & Shi, Y. (2016). Watershed model calibration to the base flow recession curve with and without evapotranspiration effects. *Water Resources Research*, 52(4), 2919–2933. doi: 10.1002/2015WR017827
- Katul, G., Manzoni, S., Palmroth, S., & Oren, R. (2009). A stomatal optimization theory to describe the effects of atmospheric CO<sub>2</sub> on leaf photosynthesis and transpiration. *Annals of Botany*, 105(3), 431–442. doi: 10.1093/aob/mcp292

- 781 Kemanian, A. R., Duckworth, P., & Williams, J. R. (2009). A spatially distributed  
782 modeling approach for precision conservation and agroecosystem design. *Proc.*  
783 *2nd Biennial Int. Symp. Farming Systems Design*, 153–154.
- 784 Kemanian, A. R., Shi, Y., White, C. M., Montes, F., Stöckle, C. O., Huggins, D. R.,  
785 ... Rozum, R. K. N. (2022). The cycles agroecosystem model: Fundamentals,  
786 testing, and applications. *Agricultural and Forest Meteorology*, *Under review*.
- 787 Kemanian, A. R., & Stöckle, C. O. (2010). C-Farm: A simple model to evaluate the  
788 carbon balance of soil profiles. *European Journal of Agronomy*, *32*(1), 22–29.  
789 doi: 10.1016/j.eja.2009.08.003
- 790 Kirchner, J. W. (2006). Getting the right answers for the right reasons: Linking  
791 measurements, analyses, and models to advance the science of hydrology. *Wa-*  
792 *ter Resources Research*, *42*(3), W03S04. doi: 10.1029/2005WR004362
- 793 Koch, J., Cornelissen, T., Fang, Z., Bogena, H., Diekkrüger, B., Kollet, S., & Stisen,  
794 S. (2016). Inter-comparison of three distributed hydrological models with re-  
795 spect to seasonal variability of soil moisture patterns at a small forested catch-  
796 ment. *Journal of Hydrology*, *533*, 234–249. doi: 10.1016/j.jhydrol.2015.12.002
- 797 Kucharik, C. J., Foley, J. A., Delire, C., Fisher, V. A., Coe, M. T., Lenters, J. D.,  
798 ... Gower, S. T. (2000). Testing the performance of a dynamic global ecosys-  
799 tem model: Water balance, carbon balance, and vegetation structure. *Global*  
800 *Biogeochemical Cycles*, *14*(3), 795–825. doi: 10.1029/1999GB001138
- 801 Kumar, M., Bhatt, G., & Duffy, C. J. (2010). An object-oriented shared data model  
802 for GIS and distributed hydrologic models. *International Journal of Geographi-*  
803 *cal Information Science*, *24*(7), 1061–1079. doi: 10.1080/13658810903289460
- 804 Leonard, L., & Duffy, C. J. (2014). Automating data-model workflows at a level 12  
805 HUC scale: Watershed modeling in a distributed computing environment. *En-*  
806 *vironmental Modelling & Software*, *61*, 174–190. doi: 10.1016/j.envsoft.2014.07  
807 .015
- 808 Lu, H., Bryant, R. B., Buda, A. R., Collick, A. S., Folmar, G. J., & Kleinman,  
809 P. J. A. (2015). Long-term trends in climate and hydrology in an agricultural,  
810 headwater watershed of central Pennsylvania, USA. *Journal of Hydrology:*  
811 *Regional Studies*, *4*, 713–731. doi: 10.1016/j.ejrh.2015.10.004
- 812 McConnell, C. A., Kaye, J. P., & Kemanian, A. R. (2020). Reviews and syntheses:  
813 Ironing out wrinkles in the soil phosphorus cycling paradigm. *Biogeosciences*,  
814 *17*(21), 5309–5333. doi: 10.5194/bg-17-5309-2020
- 815 McLellan, E. L., Cassman, K. G., Eagle, A. J., Woodbury, P. B., Sela, S., Tonitto,  
816 C., ... van Es, H. M. (2018). The Nitrogen balancing act: Tracking the envi-  
817 ronmental performance of food production. *BioScience*, *68*(3), 194–203. doi:  
818 10.1093/biosci/bix164
- 819 Molling, C. C., Strikwerda, J. C., Norman, J. M., Rodgers, C. A., Wayne, R., Mor-  
820 gan, C. L., ... Mecikalski, J. R. (2005). Distributed runoff formulation  
821 designed for a precision agricultural landscape modeling system. *Jour-*  
822 *nal of the American Water Resources Association*, *41*(6), 1289–1313. doi:  
823 10.1111/j.1752-1688.2005.tb03801.x
- 824 Pabich, W. J., Valiela, I., & Hemond, H. F. (2001). Relationship between DOC  
825 concentration and vadose zone thickness and depth below water table in  
826 groundwater of Cape Cod, U.S.A. *Biogeochemistry*, *55*(3), 247–268. doi:  
827 10.1023/A:1011842918260
- 828 PASDA. (2022). *Pennsylvania Spatial Data Access*. Retrieved 2022-04-25, from  
829 <https://www.pasda.psu.edu/>
- 830 Pineux, N., Lisein, J., Swerts, G., Bièlders, C. L., Lejeune, P., Colinet, G., & Degré,  
831 A. (2017). Can DEM time series produced by UAV be used to quantify diffuse  
832 erosion in an agricultural watershed? *Geomorphology*, *280*, 122–136. doi:  
833 10.1016/j.geomorph.2016.12.003
- 834 Pionke, H. B., Gburek, W. J., & Sharpley, A. N. (2000). Critical source area con-  
835 trols on water quality in an agricultural watershed located in the Chesapeake

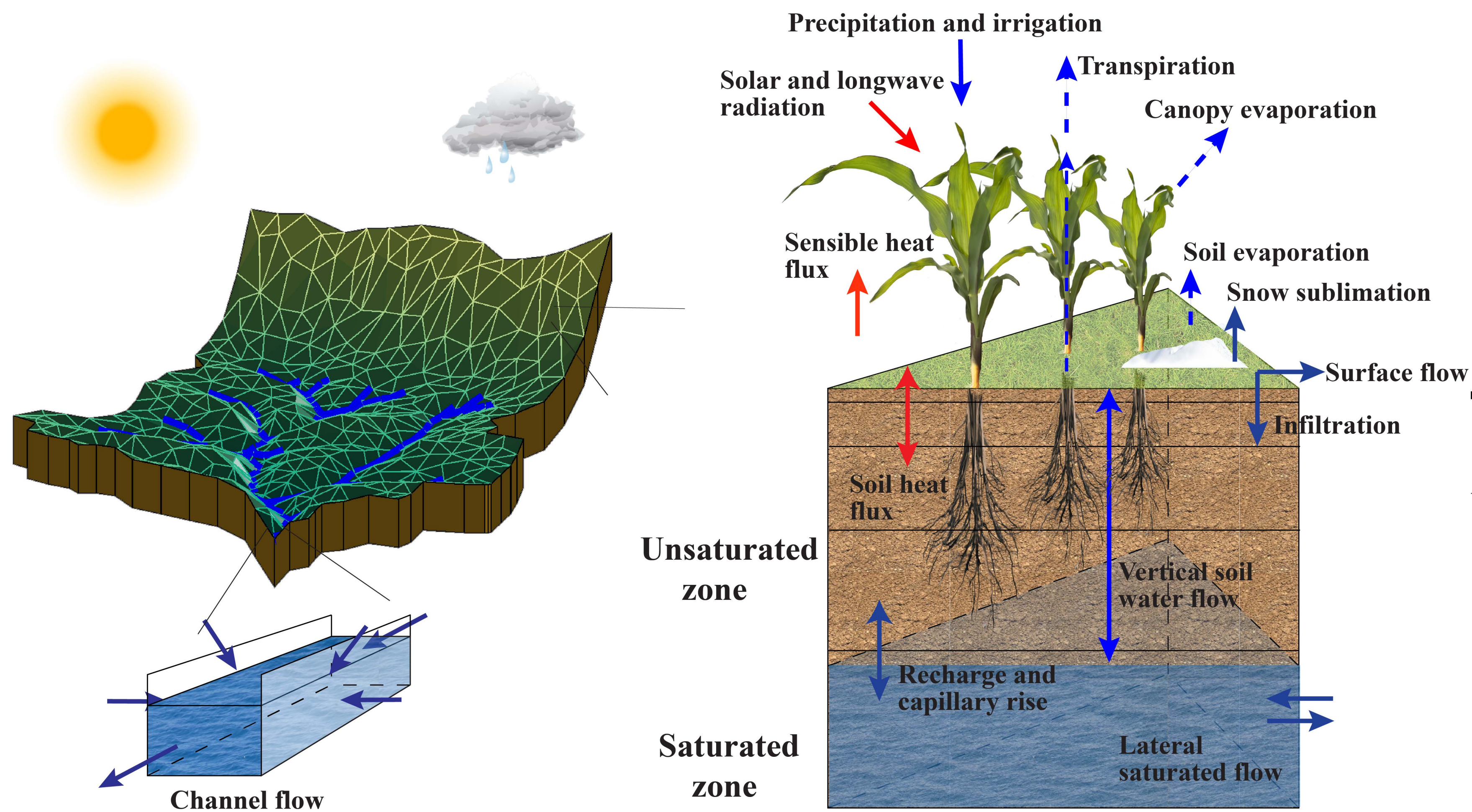
- Basin. *Ecological Engineering*, 14(4), 325–335. doi: [https://doi.org/10.1016/S0925-8574\(99\)00059-2](https://doi.org/10.1016/S0925-8574(99)00059-2)
- Pravia, M. V., Kemanian, A. R., Terra, J. A., Shi, Y., Macedo, I., & Goslee, S. (2019). Soil carbon saturation, productivity, and carbon and nitrogen cycling in crop-pasture rotations. *Agricultural Systems*, 171(December 2017), 13–22. doi: 10.1016/j.agsy.2018.11.001
- Qu, Y., & Duffy, C. J. (2007). A semidiscrete finite volume formulation for multiprocess watershed simulation. *Water Resources Research*, 43(8), W08419. doi: 10.1029/2006WR005752
- Redder, B. W., Kennedy, C. D., Buda, A. R., Folmar, G., & Boyer, E. W. (2021). Groundwater contributions of flow and nitrogen in a headwater agricultural watershed. *Hydrological Processes*, 35(5), e14179. doi: 10.1002/hyp.14179
- Rodell, M., Houser, P. R., Jambor, U., Gottschalck, J., Mitchell, K., Meng, C.-J., . . . Others (2004). The global land data assimilation system. *Bulletin of the American Meteorological Society*, 85(3), 381–394. doi: 10.1175/BAMS-85-3-381
- Saarikko, R. A. (2000). Applying a site based crop model to estimate regional yields under current and changed climates. *Ecological Modelling*, 131(2), 191–206. doi: 10.1016/S0304-3800(00)00257-X
- Saha, D., Kaye, J. P., Bhowmik, A., Bruns, M. A., Wallace, J. M., & Kemanian, A. R. (2021). Organic fertility inputs synergistically increase denitrification-derived nitrous oxide emissions in agroecosystems. *Ecological Applications*, 31(7), e02403. doi: 10.1002/eap.2403
- Saha, D., Rau, B. M., Kaye, J. P., Montes, F., Adler, P. R., & Kemanian, A. R. (2017). Landscape control of nitrous oxide emissions during the transition from conservation reserve program to perennial grasses for bioenergy. *GCB Bioenergy*, 9(4), 783–795. doi: 10.1111/gcbb.12395
- Shi, Y., Baldwin, D. C., Davis, K. J., Yu, X., Duffy, C. J., & Lin, H. (2015). Simulating high-resolution soil moisture patterns in the Shale Hills watershed using a land surface hydrologic model. *Hydrological Processes*, 29(21), 4624–4637. doi: 10.1002/hyp.10593
- Shi, Y., Davis, K. J., Duffy, C. J., & Yu, X. (2013). Development of a Coupled Land Surface Hydrologic Model and Evaluation at a Critical Zone Observatory. *Journal of Hydrometeorology*, 14(5), 1401–1420. doi: 10.1175/JHM-D-12-0145.1
- Shi, Y., Davis, K. J., Zhang, F., & Duffy, C. J. (2014). Evaluation of the Parameter Sensitivities of a Coupled Land Surface Hydrologic Model at a Critical Zone Observatory. *Journal of Hydrometeorology*, 15(1), 279–299. doi: 10.1175/JHM-D-12-0177.1
- Shi, Y., Eissenstat, D. M., He, Y., & Davis, K. J. (2018). Using a spatially-distributed hydrologic biogeochemistry model with a nitrogen transport module to study the spatial variation of carbon processes in a Critical Zone Observatory. *Ecological Modelling*, 380, 8–21. doi: 10.1016/j.ecolmodel.2018.04.007
- Stafford, J. V. (2000). Implementing precision agriculture in the 21st century. *Journal of Agricultural and Engineering Research*, 76(3), 267–275. doi: 10.1006/jaer.2000.0577
- Stöckle, C. O., & Kemanian, A. R. (2020). Can crop models identify critical gaps in genetics, environment, and management interactions? *Frontiers in Plant Science*, 11, 737. doi: 10.3389/fpls.2020.00737
- Stöckle, C. O., Kemanian, A. R., Nelson, R. L., Adam, J. C., Sommer, R., & Carlson, B. (2014). CropSyst model evolution: From field to regional to global scales and from research to decision support systems. *Environmental Modelling & Software*, 62, 361–369. doi: 10.1016/j.envsoft.2014.09.006
- Tague, C. L., & Band, L. E. (2004). RHESSys: Regional Hydro-Ecologic Simulation System—An object-oriented approach to spatially distributed modeling of carbon, water, and nutrient cycling. *Earth Interactions*, 8(19), 1–42. doi:

- 10.1175/1087-3562(2004)8<1:RRHSSO>2.0.CO;2
- 891 Tarboton, D. G. (2015). *TauDEM -Terrain Analysis Using Digital Elevation Models.*  
892 *Version 5.* Retrieved 2022-04-25, from [https://hydrology.usu.edu/taudem/](https://hydrology.usu.edu/taudem/taudem5/index.html)  
893 [taudem5/index.html](https://hydrology.usu.edu/taudem/taudem5/index.html)  
894
- 895 Tarboton, D. G., Bras, R. L., & Rodriguez-Iturbe, I. (1991). On the extraction of  
896 channel networks from digital elevation data. *Hydrological Processes*, *5*(1), 81–  
897 100. doi: 10.1002/hyp.3360050107
- 898 Tarboton, D. G., Schreuders, K. A. T., Watson, D. W., & Baker, M. E. (2009). Gen-  
899 eralized terrain-based flow analysis of digital elevation models. In *Proceedings*  
900 *of the 18th world imacs congress and modsim09 international congress on mod-*  
901 *elling and simulation, cairns, australia* (Vol. 20002006, pp. 2377–2383). Cairns,  
902 Australia.
- 903 Tenreiro, T. R., García-Vila, M., Gómez, J. A., Jimenez-Berni, J. A., & Fereres, E.  
904 (2020). Water modelling approaches and opportunities to simulate spatial wa-  
905 ter variations at crop field level. *Agricultural Water Management*, *240*, 106254.  
906 doi: 10.1016/j.agwat.2020.106254
- 907 USDA-NRCS. (2012). *Assessment of the effects of conservation practices on cul-*  
908 *tivated cropland in the Upper Mississippi River Basin (Revised CEAP Report*  
909 *2012)* (Tech. Rep.).
- 910 Van Liew, M. W., Wortmann, C. S., Moriasi, D. N., King, K. W., Flanagan, D. C.,  
911 Veith, T. L., ... Tomer, M. D. (2017). Evaluating the APEX model for simu-  
912 lating streamflow and water quality on ten Agricultural watersheds in the U.S.  
913 *Transactions of the American Society of Agricultural and Biological Engineers*,  
914 *60*(1), 123–146. doi: 10.13031/trans.11903
- 915 Veith, T. L., Richards, J. E., Goslee, S. C., Collick, A. S., Bryant, R. B., Miller,  
916 D. A., ... Kleinman, P. J. (2015). Navigating spatial and temporal com-  
917 plexity in developing a long-term land use database for an agricultural wa-  
918 tershed. *Journal of Soil and Water Conservation*, *70*(5), 288–296. doi:  
919 10.2489/jswc.70.5.288
- 920 Wallace, C. D., Sawyer, A. H., Soltanian, M. R., & Barnes, R. T. (2020). Nitrate re-  
921 moval within heterogeneous riparian aquifers under tidal influence. *Geophysical*  
922 *Research Letters*, *47*(10), e2019GL085699. doi: 10.1029/2019GL085699
- 923 Wang, C., Hou, J., Miller, D., Brown, I., & Jiang, Y. (2019). Flood risk management  
924 in sponge cities: The role of integrated simulation and 3D visualization. *Inter-*  
925 *national Journal of Disaster Risk Reduction*, *39*, 101139. doi: 10.1016/j.ijdr  
926 .2019.101139
- 927 Wang, X., Kemanian, A. R., & Williams, J. R. (2011). Special features of the EPIC  
928 and APEX modeling package and procedures for parameterization, calibration,  
929 validation, and applications. In L. R. Ahuja & L. Ma (Eds.), *Methods of intro-*  
930 *ducing system models into agricultural research* (pp. 177–208). John Wiley &  
931 Sons, Ltd. doi: 10.2134/advagricsystmodel2.c6
- 932 Ward, N. K., Maureira, F., Stöckle, C. O., Brooks, E. S., Painter, K. M., Yourek,  
933 M. A., & Gasch, C. K. (2018). Simulating field-scale variability and preci-  
934 sion management with a 3D hydrologic cropping systems model. *Precision*  
935 *Agriculture*, *19*(2), 293–313. doi: 10.1007/s11119-017-9517-6
- 936 Wigmosta, M. S., & Lettenmaier, D. P. (1999). A comparison of simplified methods  
937 for routing topographically driven subsurface flow. *Water Resources Research*,  
938 *35*(1), 255–264. doi: 10.1029/1998WR900017
- 939 Williams, J. R. (1990). The Erosion-Productivity Impact Calculator (EPIC) model:  
940 A case history. *Philosophical Transactions of the Royal Society of London. Se-*  
941 *ries B: Biological Sciences*, *329*(1255), 421–428. doi: 10.1098/rstb.1990.0184
- 942 Williams, M. R., Buda, A. R., Elliott, H. A., Singha, K., & Hamlett, J. (2015).  
943 Influence of riparian seepage zones on nitrate variability in two agricultural  
944 headwater streams. *Journal of the American Water Resources Association*  
945 (*JAWRA*), *51*(4), 883–897. doi: 10.1111/1752-1688.12335

- 946 Woodbury, P. B., Kemanian, A. R., Jacobson, M., & Langholtz, M. (2018). Im-  
 947 proving water quality in the Chesapeake Bay using payments for ecosystem  
 948 services for perennial biomass for bioenergy and biofuel production. *Biomass*  
 949 *and Bioenergy*, *114*, 132–142. doi: 10.1016/j.biombioe.2017.01.024
- 950 Xia, Y., Mitchell, K., Ek, M., Sheffield, J., Cosgrove, B., Wood, E., . . . Mocko,  
 951 D. (2012, feb). Continental-scale water and energy flux analysis and valida-  
 952 tion for the North American Land Data Assimilation System project phase 2  
 953 (NLDAS-2): 1. Intercomparison and application of model products. *Journal of*  
 954 *Geophysical Research*, *117*, D03109. doi: 10.1029/2011JD016048
- 955 Xiao, D., Shi, Y., Brantley, S. L., Forsythe, B., DiBiase, R., Davis, K., & Li, L.  
 956 (2019). Streamflow generation from catchments of contrasting lithologies:  
 957 The role of soil properties, topography, and catchment size. *Water Resources*  
 958 *Research*, *55*(11), 9234–9257. doi: 10.1029/2018WR023736
- 959 Zhai, Z., Martínez, J. F., Beltran, V., & Martínez, N. L. (2020). Decision support  
 960 systems for agriculture 4.0: Survey and challenges. *Computers and Electronics*  
 961 *in Agriculture*, *170*, 105256. doi: 10.1016/j.compag.2020.105256
- 962 Zhang, Y., Li, W., Sun, G., Miao, G., Noormets, A., Emanuel, R., & King, J. S.  
 963 (2018). Understanding coastal wetland hydrology with a new regional-scale,  
 964 process-based hydrological model. *Hydrological Processes*, *32*(20), 3158–3173.  
 965 doi: 10.1002/hyp.13247
- 966 Zheng, W., Lamačová, A., Yu, X., Krám, P., Hruška, J., Zahradníček, P., . . . Farda,  
 967 A. (2021). Assess hydrological responses to a warming climate at the Lysina  
 968 Critical Zone Observatory in Central Europe. *Hydrological Processes*, *35*(9),  
 969 e14281. doi: 10.1002/hyp.14281
- 970 Zhi, W., Shi, Y., Wen, H., Saberi, L., Ng, G.-H. C., Sadayappan, K., . . . Li, L.  
 971 (2022). BioRT-Flux-PIHM v1.0: A biogeochemical reactive transport model at  
 972 the watershed scale. *Geoscientific Model Development*, *15*(1), 315–333. doi:  
 973 10.5194/gmd-15-315-2022

Figure 1.

# Flux-PIHM



**Daily meteorological condition**  
**Soil temperature**  
**Soil moisture**  
**Snow cover**  
**Vertical soil water flow**  
**Lateral saturated flow**



**Evapotranspiration**  
**(replaces corresponding functions in Flux-PIHM)**

# Cycles

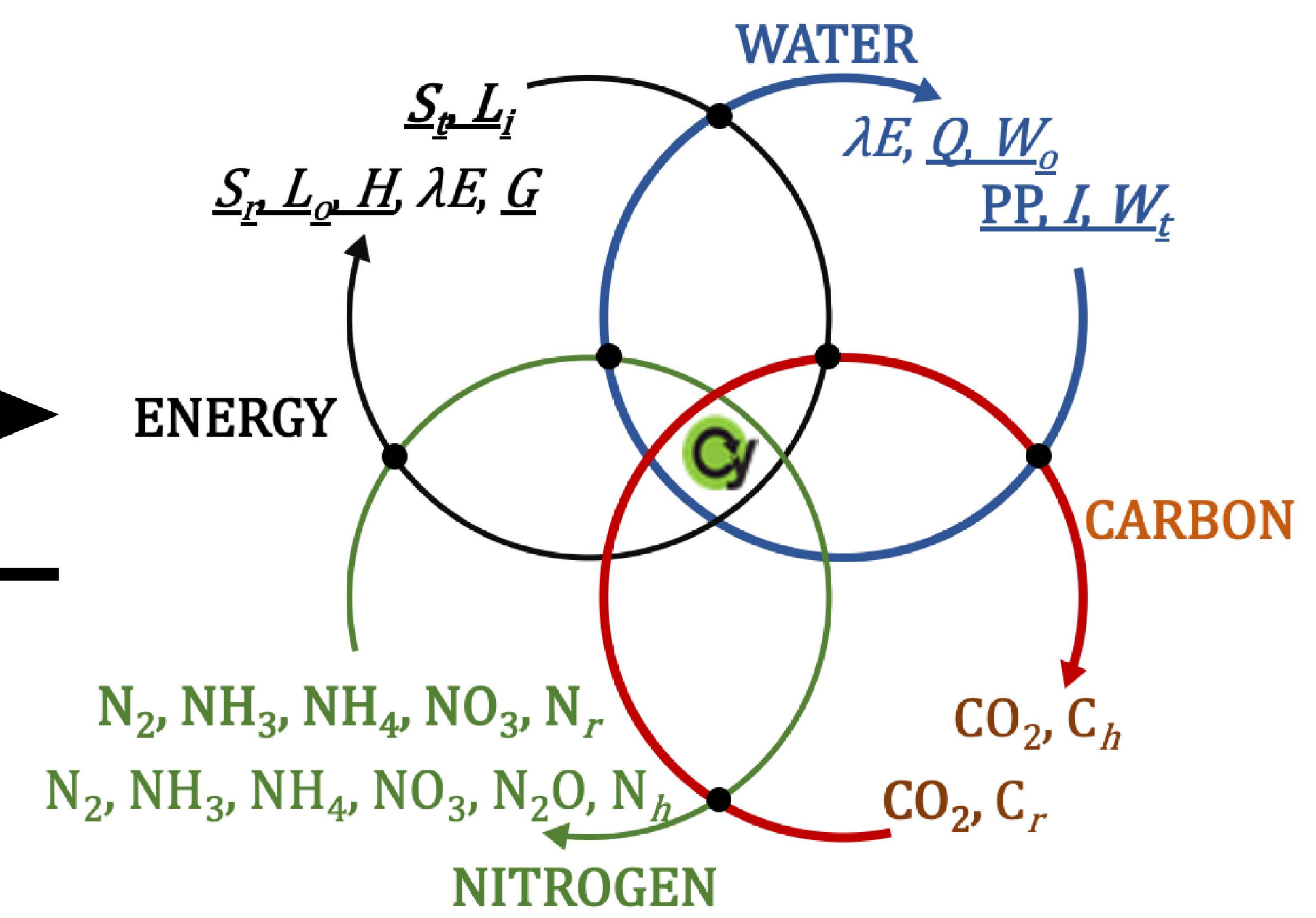


Figure 2.

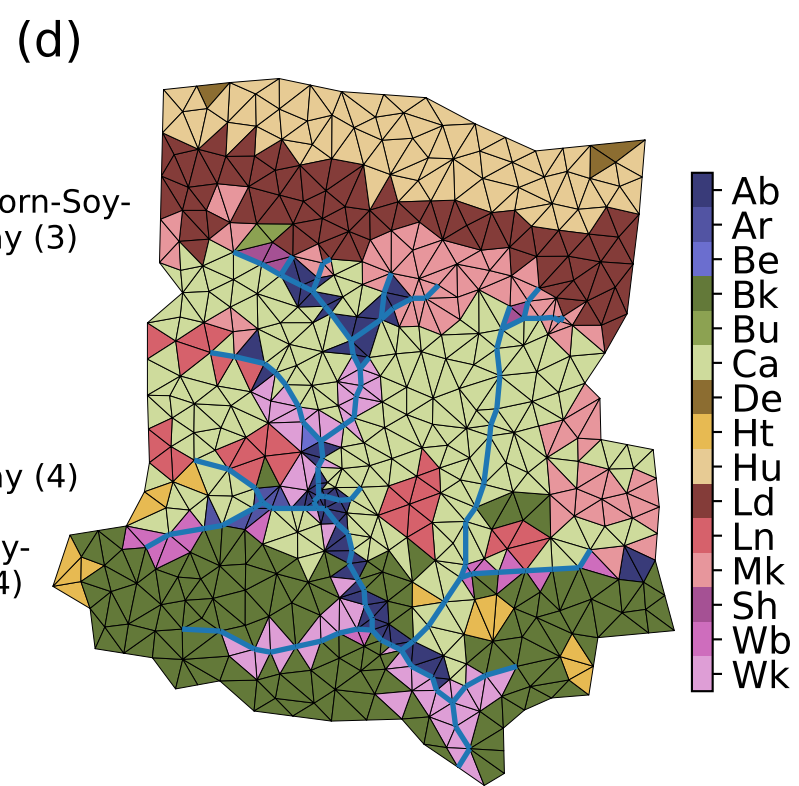
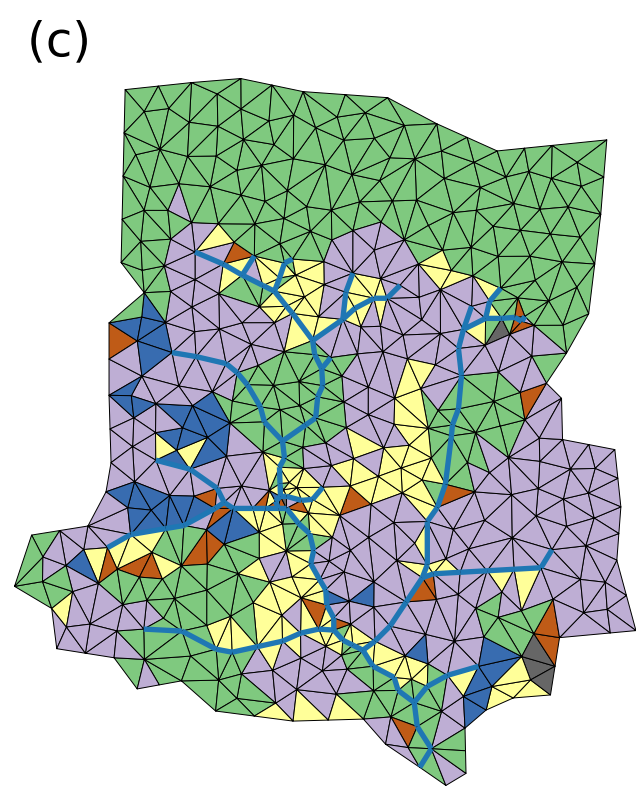
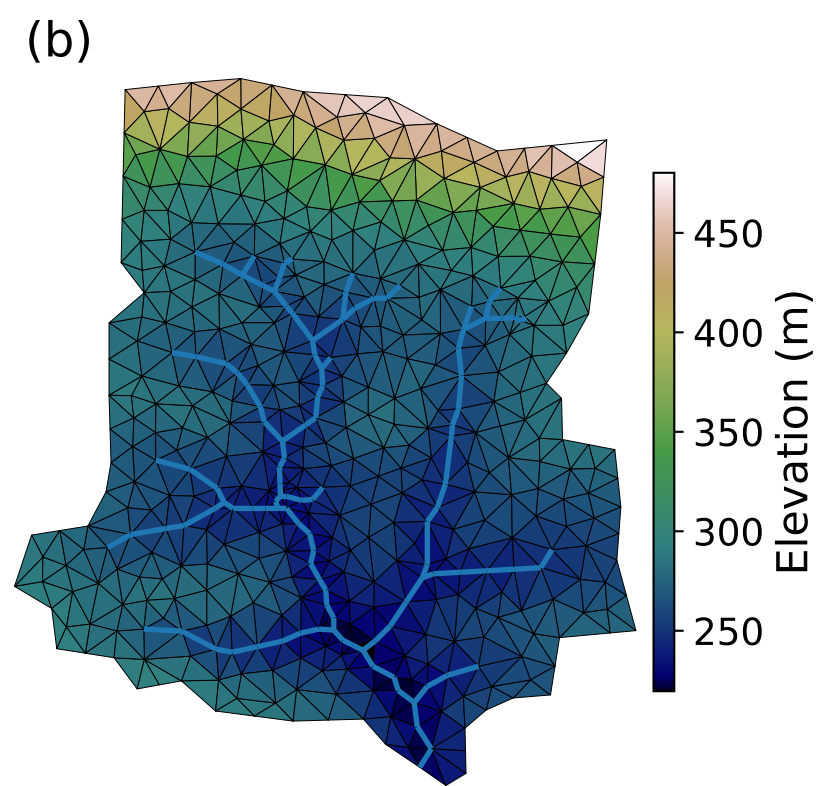
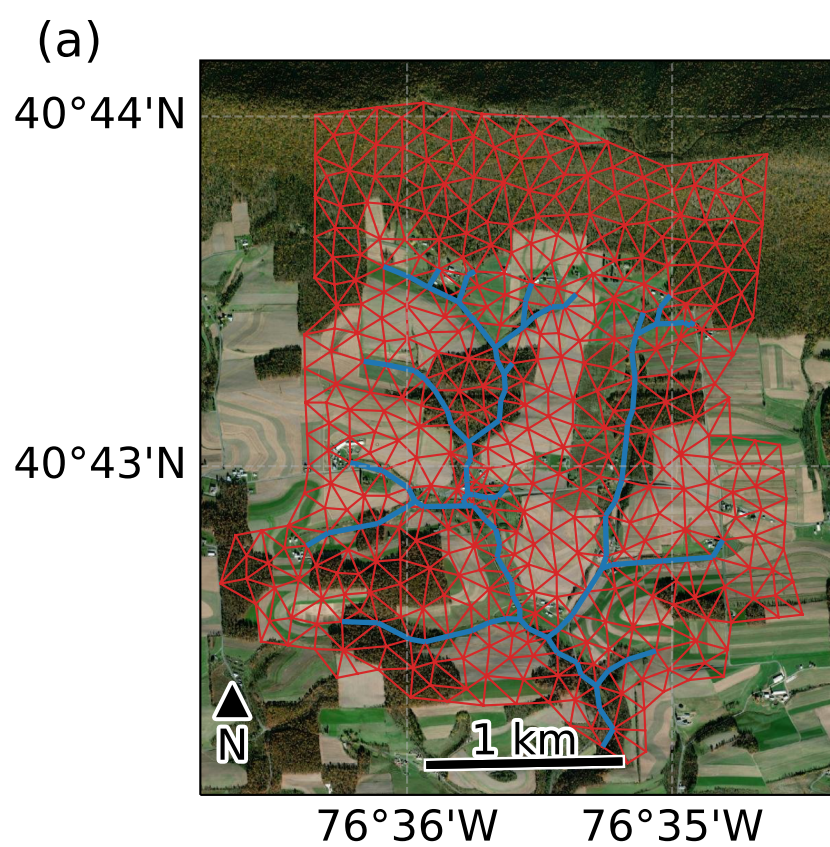


Figure 3.

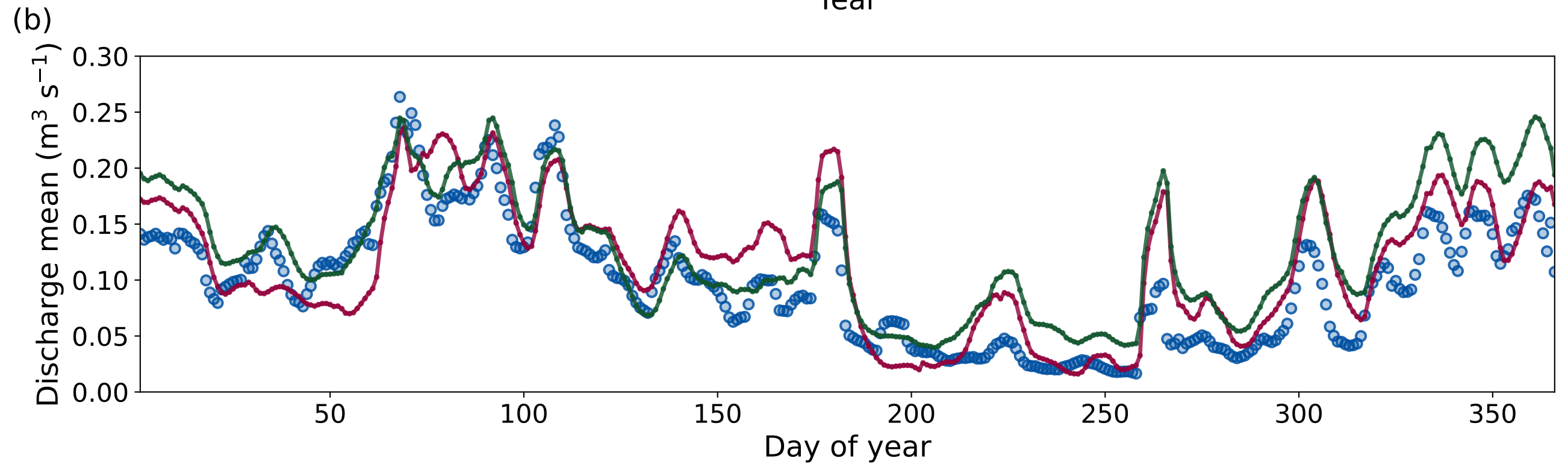
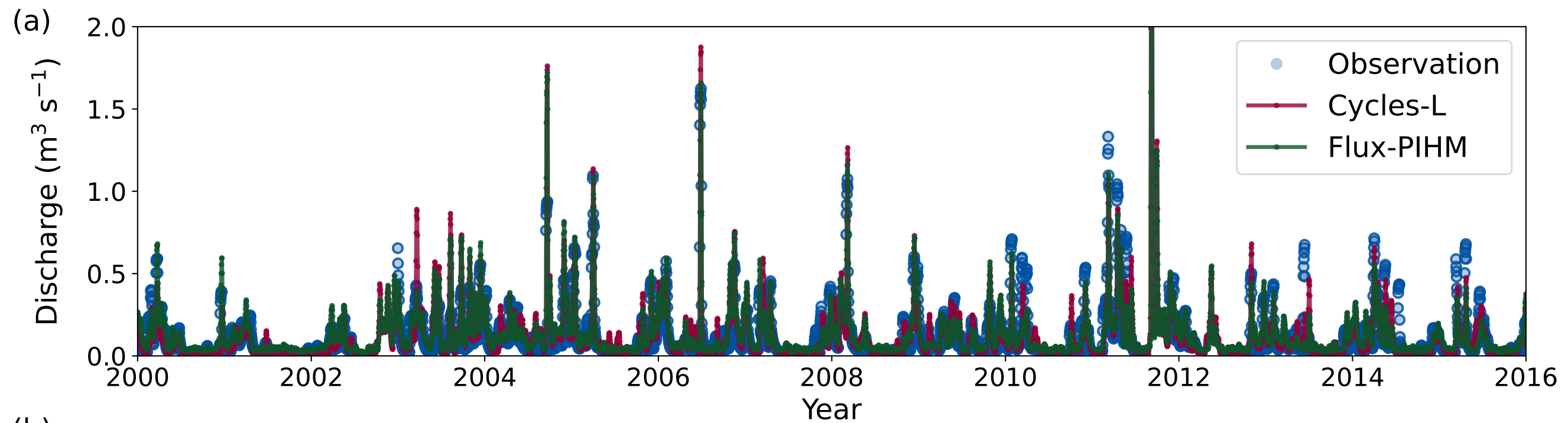


Figure 4.

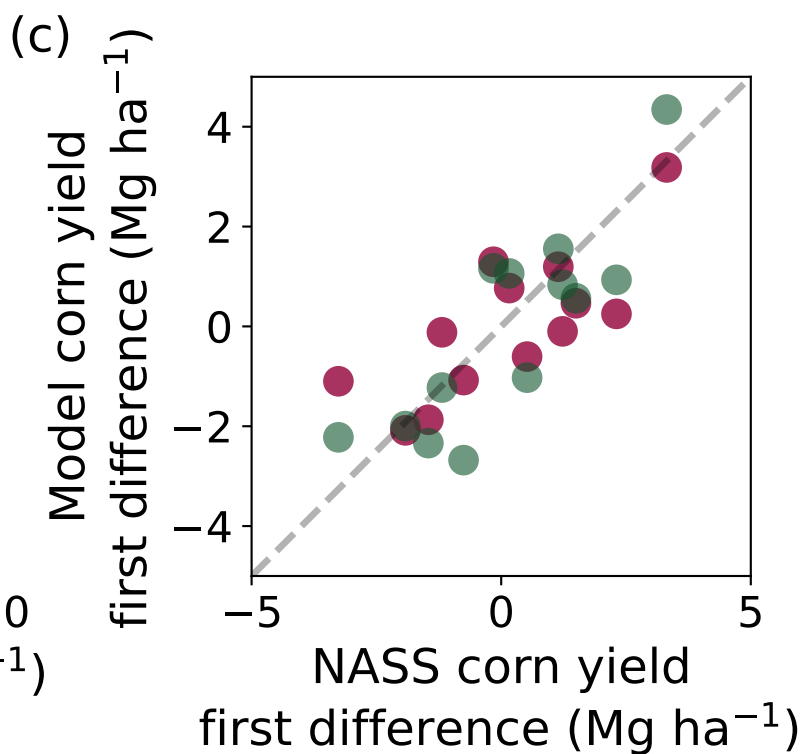
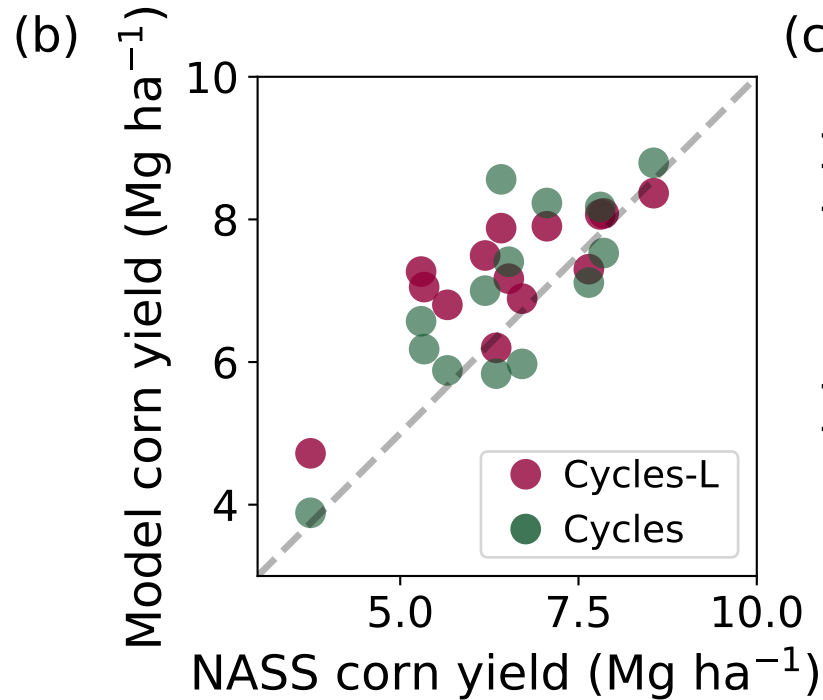
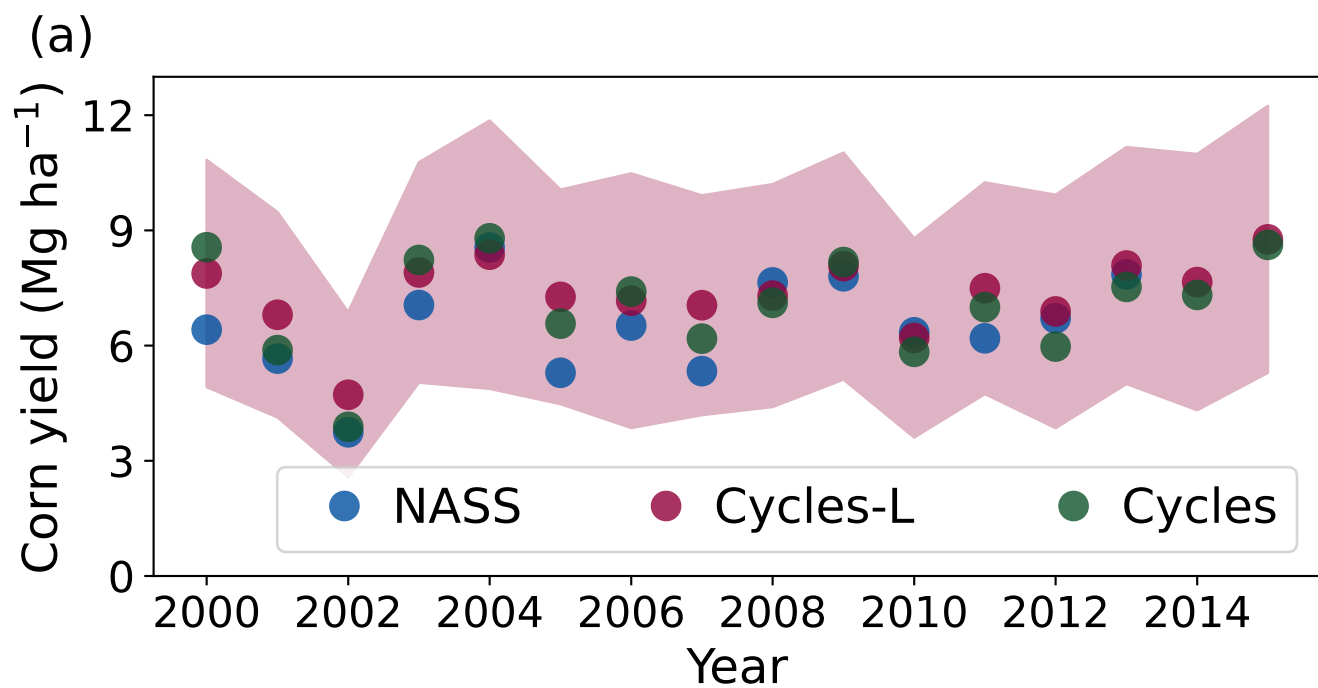


Figure 5.

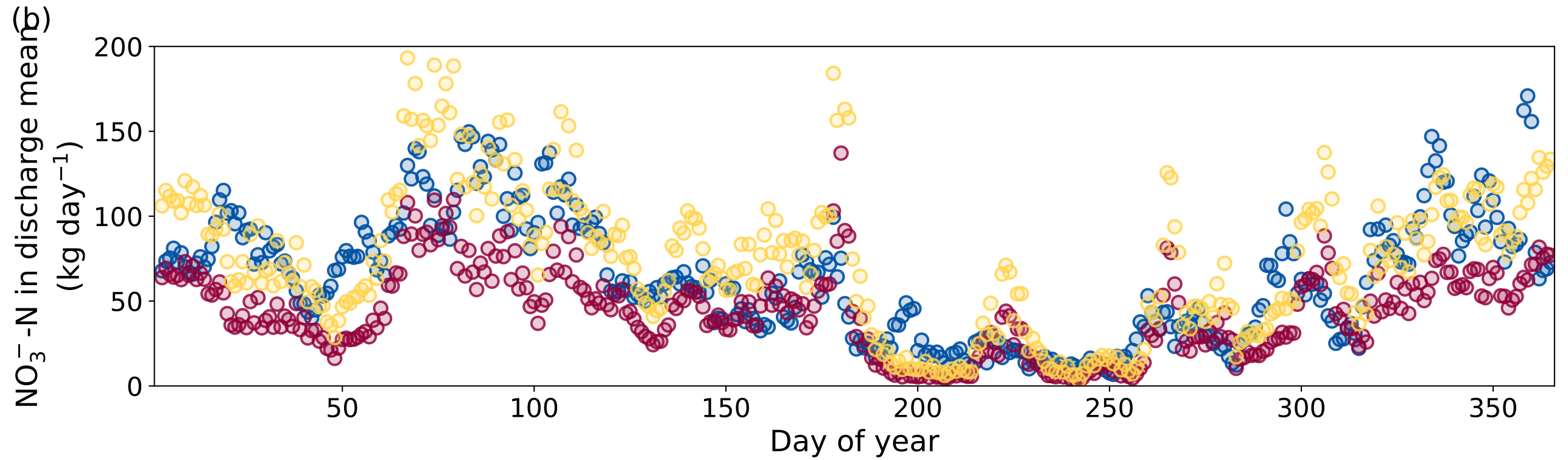
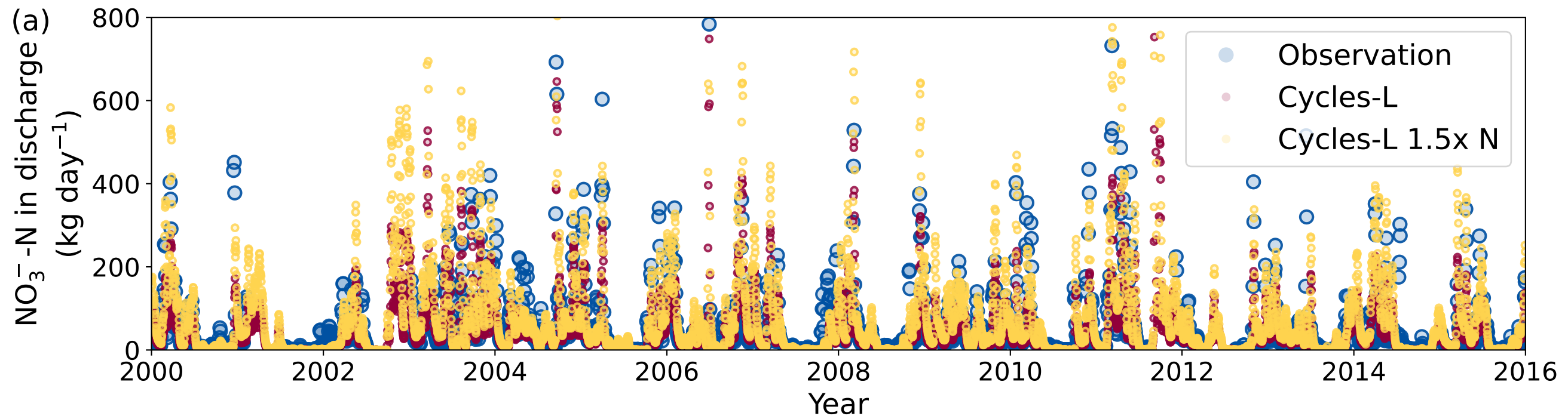


Figure 6.

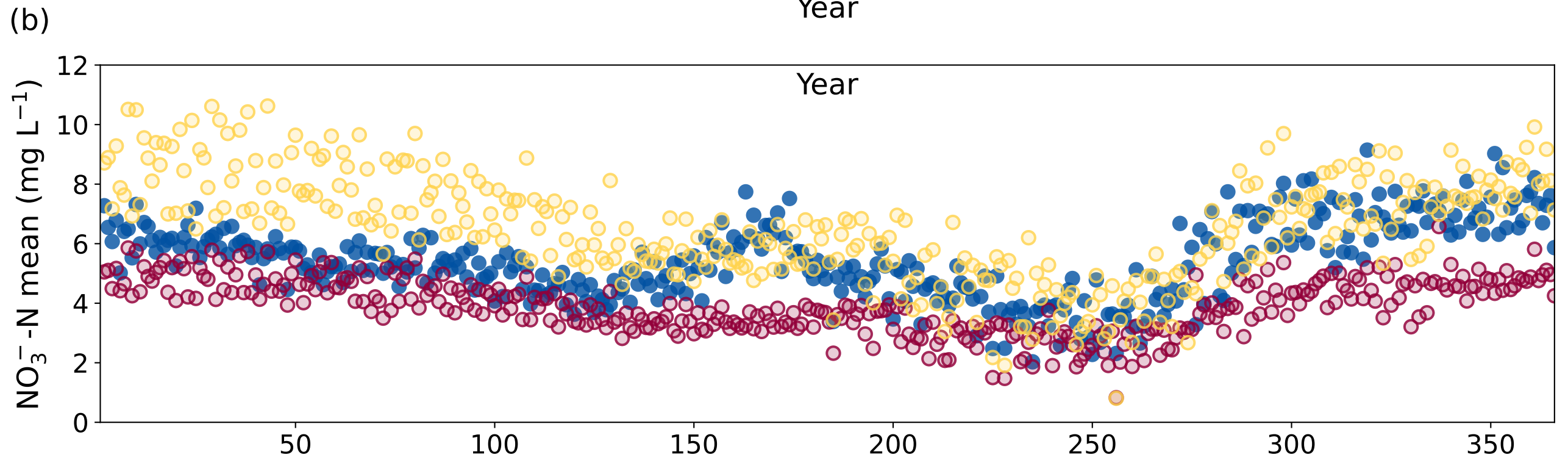
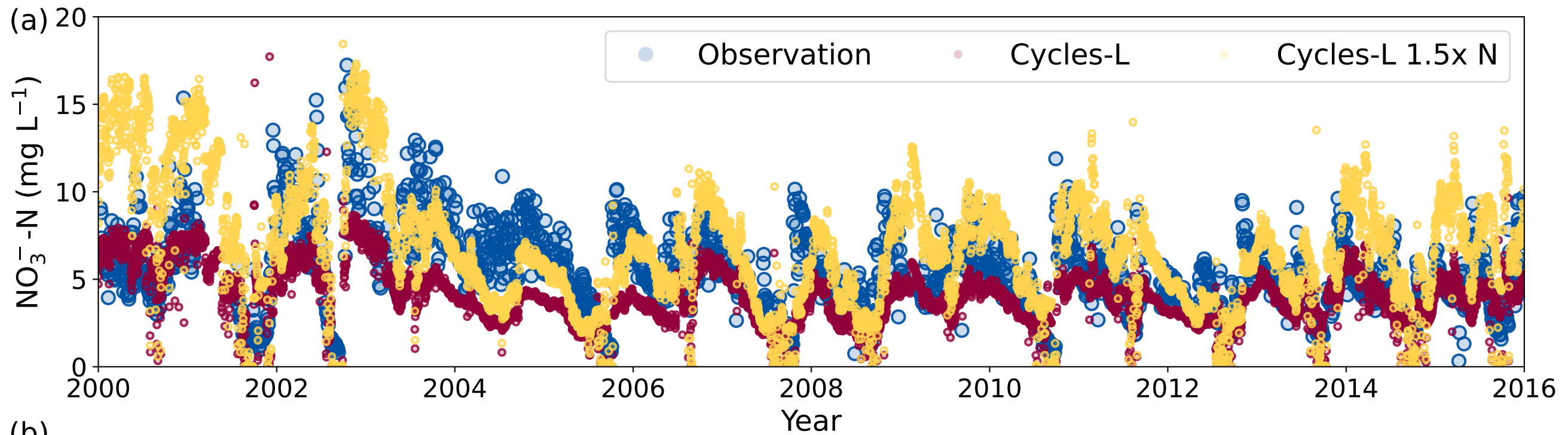


Figure 7.

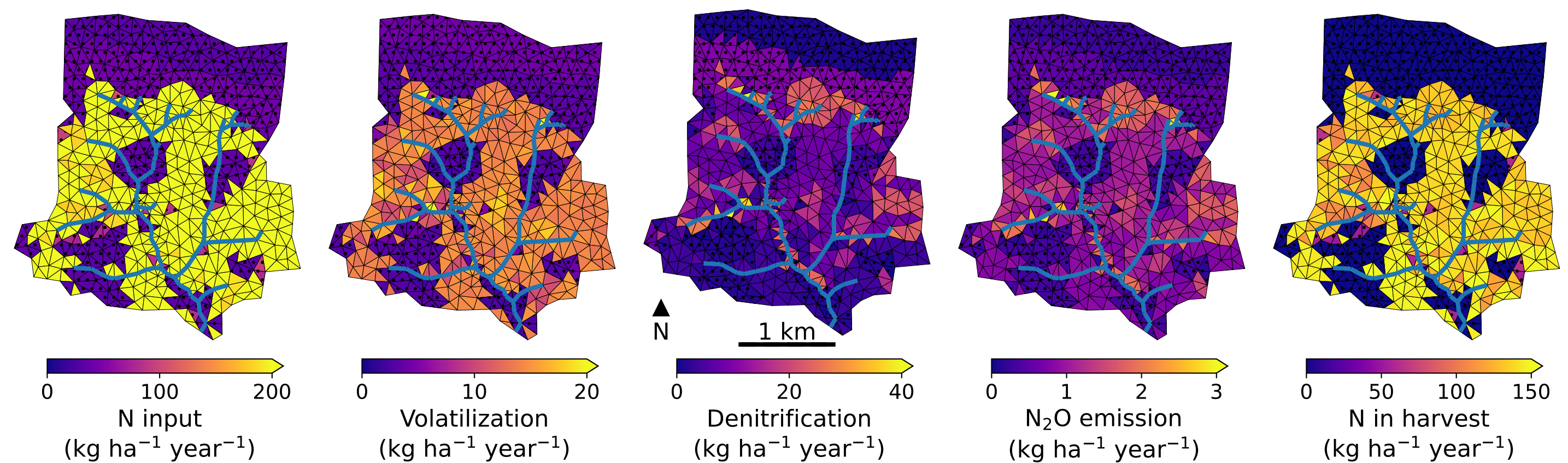


Figure 8.

